# The LCLAT1/LYCAT acyltransferase supports EGF-mediated phosphatidylinositol-3,4,5-trisphosphate and Akt signaling

Victoria Chan[1,2], Leslie Bone[1,2], Karen E. Anderson[3], Kai Zhang[2], Laura Orofiamma[1,2], Yasmin Awadeh[1,2], Daniel K. C. Lee[4], Norman J. Fu[4], Jonathan T. S. Chow[4], Leonardo Salmena[4], Len R. Stephens[3], Phillip T. Hawkins[3], Costin N. Antonescu[1,2]*, and Roberto J. Botelho[1,2]*

[1]Molecular Science Graduate Program and [2]Department of Chemistry and Biology, Toronto Metropolitan University, Toronto, Ontario, M5B2K3, Canada

[3]Inositide Laboratory, Babraham Institute, Cambridge CB22 4AT, United Kingdom

[4]Department of Pharmacology & Toxicology, University of Toronto, Toronto, Ontario, M5S1A8, Canada

***Correspondence should be sent to:**

Costin N. Antonescu: cantonescu@torontomu.ca and Roberto J. Botelho: rbotelho@torontomu.ca

**Running title:** LCLAT1 acyltransferase and PtdIns(3,4,5) $P_3$-Akt

**Keywords**: cancer, cell signaling, lipids, kinase, phosphorylation, growth factor, cell proliferation

**Abbreviations:** BSA: bovine serum albumin; EGF: epidermal growth factor: EGFR: epidermal growth factor receptor; $IP_3$: inositol-1,4,5-trisphosphate; ER: endoplasmic reticulum; PtdIns: phosphatidylinositol; PtdIns(3)P: phosphatidylinositol-3-phosphate; PtdIns(4,5)$P_2$: phosphatidylinositol-4,5-bisphosphate; PtdIns(3,4,5)$P_3$: phosphatidylinositol-3,4,5-trisphosphate; PtdInsP: phosphoinositide; TIRF: total internal reflection fluorescence; TNBC: triple negative breast cancer

**Abstract**

Receptor tyrosine kinases such as epidermal growth factor (EGF) receptor (EGFR) stimulate phosphatidylinositol 3-kinases (PI3Ks) to convert phosphaitydlinositol-4,5-bisphosophate [PtdIns(4,5)$P_2$] into phosphatidylinositol-3,4,5-trisphosphate [PtdIns(3,4,5)$P_3$]. PtdIns(3,4,5)$P_3$ then promotes various pathways leading to actin remodelling, changes in gene expression, and enhanced anabolic activity, cell survival and proliferation. In part, PtdIns(3,4,5)$P_3$ achieves these functions by stimulating the kinase Akt, which phosphorylates numerous targets like Tsc2 and GSK3β. Overall, unchecked upregulation of PtdIns(3,4,5)$P_3$-Akt signalling can promote tumourgenesis and cancer progression. Interestingly, 50-70% of PtdIns and PtdInsPs have stearate and arachidonate at *sn*-1 and *sn*-2 positions of glycerol, respectively, forming a species known as 38:4-PtdIns/PtdInsPs. It is thought that LCLAT1/LYCAT and MBOAT7/LPIAT1 acyltransferases are respectively responsible for enriching PtdIns with this acyl composition. We previously showed that disruption of LCLAT1 altered the acyl profile of bis-phosphorylated PtdInsPs, lowered PtdIns(4,5)$P_2$, and perturbed endocytosis and endocytic trafficking. However, the role of LCLAT1 in receptor tyrosine kinase and PtdIns(3,4,5)$P_3$ signaling was not explored. Here, we show that LCLAT1 silencing in MDA-MB-231 and ARPE-19 cells abated the levels of PtdIns(3,4,5)$P_3$ in response to EGF signalling. Importantly, LCLAT1-silenced cells were also impaired for EGF-mediated Akt activation and downstream signalling, and consequently, were depressed for cell proliferation and survival. Thus, our work provides first evidence that the LCLAT1 acyltransferase supports receptor tyrosine kinase signalling through the PtdIns(3,4,5)$P_3$-Akt axis and may represent a novel target for therapeutic development against cancers.

## Introduction

Phosphoinositide (PtdInsP) lipid signaling orchestrates a variety of cellular functions such as organelle identity and membrane trafficking, ion channel activity, cytoskeletal organization, regulation of gene expression, modulation of metabolic activity, and cell proliferation and survival (Balla, 2013; Choy et al., 2017; Dickson and Hille, 2019; Doumane et al., 2022; Idevall-Hagren and De Camilli, 2015; Posor et al., 2022). PtdInsPs are generated by the reversible phosphorylation of the phosphatidylinositol (PtdIns) headgroup by several types of lipid kinases and phosphatases. Collectively, and based on the headgroup phosphorylation, these enzymes can generate up to seven species of PtdInsPs (Balla, 2013; Choy et al., 2017; Dickson and Hille, 2019; Posor et al., 2022). Nonetheless, there is another facet of PtdInsP biology that is poorly defined at the regulatory and functional levels – the control and function of the acyl composition of PtdInsPs (Barneda et al., 2019; Bozelli and Epand, 2019; Choy et al., 2017; D'Souza and Epand, 2014; Traynor-Kaplan et al., 2017).

In many mammalian tissues and cells, 50-70% of PtdIns and PtdInsPs are enriched for stearate and arachidonate at the *sn*-1 and *sn*-2 positions, respectively – this acyl combination is referred to as 38:4-PtdIns or 38:4-PtdInsPs (Anderson et al., 2013; Anderson et al., 2016; Barneda et al., 2019; D'Souza and Epand, 2014; Haag et al., 2012; Imae et al., 2012; Lee et al., 2012; Milne et al., 2005; Traynor-Kaplan et al., 2017). Additionally, this acyl composition is unique to PtdIns and PtdInsPs – other phospholipids have distinct acyl profiles (Barneda et al., 2019; Bozelli and Epand, 2019; Hicks et al., 2006; Traynor-Kaplan et al., 2017). This suggests that the acyl groups of PtdIns and PtdInsPs play a more significant role than simply embedding the lipids into the membrane bilayer (Barneda et al., 2019; Bozelli and Epand, 2019; Choy et al.,

2017). However, while there is an enrichment for 38:4 species, the exact acyl profile of PtdIns and PtdInsPs can vary between cell types, environmental conditions and stresses, and patho-physiological conditions like cancer (Anderson et al., 2016, 10; Barneda et al., 2019; Bozelli and Epand, 2019; Hicks et al., 2006; Imae et al., 2012; Mujalli et al., 2018; Traynor-Kaplan et al., 2017). For example, $p53^{-/-}$ cancer cells, prostate cancer cells and triple negative breast cancer tissue all have distinct acyl profiles of PtdIns relative to normal tissue (Freyr Eiriksson et al., 2020; Koizumi et al., 2019; Naguib et al., 2015; Rueda-Rincon et al., 2015). Yet, there is much to be understood about the regulatory mechanisms that establish and remodel the acyl profile of PtdIns and PtdInsPs, and their functional implications.

The LCLAT1 acyltransferase has been identified as one of the enzymes that remodels and enriches PtdIns and/or PtdInsPs in stearate at the *sn*-1 position (Bone et al., 2017; D'Souza and Epand, 2014; Imae et al., 2012). LCLAT1 is an ER-localized protein and is thought to act during the Lands' Cycle or PtdIns Cycle to enrich PtdIns in stearate at *sn*-1, though this remains partially undefined or even assumed (Barneda et al., 2019; Blunsom and Cockcroft, 2020; Bone et al., 2017; Imae et al., 2012). Disruption of LCLAT1 has been shown to reduce the levels of 38:4-PtdIns, mono-PtdInsP, and bis-phosphorylated PtdInsPs in mouse tissues like in brain tissue (Imae et al., 2012). More recently, we showed that LCLAT1 silencing had a more specific effect in ARPE-19 cells, a non-transformed human retinal epithelium cell line (Bone et al., 2017). We observed that LCLAT1 silencing reduces the relative levels of endosomal phosphatidylinositol-3-phosphate [PtdIns(3)P] and phosphatidylinositol-4,5-bisphosphate [PtdIns(4,5)$P_2$] on the plasma membrane, but not phosphatidylinositol-4-phosphate [PtdIns(4)P] (Bone et al., 2017). Importantly, PtdIns and bis-phosphorylated PtdInsPs (mostly PtdIns(4,5)$P_2$), but not mono-phosphorylated PtdInsPs (mostly PtdIns(4)P] were altered in their acyl profile upon LCLAT1

silencing. This effect on specific pools of PtdInsPs has also been observed in cells disrupted for LPIAT1/MBOAT7, an acyltransferase thought to enrich PtdIns/PtdInsPs in arachidonic acid (Anderson et al., 2013).

PtdIns(4,5)$P_2$ regulates a number of functions including endocytosis, ion transport, and the cytoskeleton organization (Balla, 2013; Katan and Cockcroft, 2020; Sun et al., 2013). PtdIns(4,5)$P_2$ is also a precursor for other signalling intermediates regulated by growth factor receptors like the Epidermal Growth Factor (EGF) and its receptor, the EGF receptor (EGFR), a major receptor tyrosine kinase (Katan and Cockcroft, 2020; Orofiamma et al., 2022). EGF binds and dimerizes EGFR, leading to receptor trans-autophosphorylation on various tyrosine residues (Böni-Schnetzler and Pilch, 1987; Gullick et al., 1985; Honegger et al., 1987; Koland and Cerione, 1988; Linggi and Carpenter, 2006; Yarden and Schlessinger, 1987). These phospho-tyrosines serve as docking sites for adaptor proteins like Gab1 and Grb2, which assemble a signaling complex composed of other protein kinases and phosphatases, and lipid-metabolizing enzymes (Holgado-Madruga et al., 1996, 2; Margolis et al., 1990a; Orofiamma et al., 2022; Rodrigues et al., 2000). For example, active EGFR recruits and activates Phospholipase Cγ (PLCγ), which hydrolyses PtdIns(4,5)$P_2$ into diacylglycerol and inositol-1,4,5-trisphosphate ($IP_3$), and which releases $Ca^{2+}$ from endoplasmic reticulum stores (Delos Santos et al., 2017; Margolis et al., 1990a; Margolis et al., 1990b). In addition, Gab1 recruits the Class I PI3Ks to convert PtdIns(4,5)$P_2$ to PtdIns(3,4,5)$P_3$ (Kiyatkin et al., 2006; Rodrigues et al., 2000). This burst of PtdIns(3,4,5)$P_3$ then recruits and activates PDK1 and Akt protein kinases (Alessi et al., 1997; Bellacosa et al., 1998; Manning and Toker, 2017; Stokoe et al., 1997). Akt is a major driver of cell metabolism and growth by phosphorylating numerous targets like GSK3β and TSC2 (Cross et al., 1995; Inoki et al., 2002; Manning and Toker, 2017; Rodgers et al., 2017; Sugiyama et al.,

2019). For example, Akt inactivates TSC2, a GTPase activating protein (GAP) for the Rheb GTPase, thus promoting the mTORC1 pathway (Inoki et al., 2002; Inoki et al., 2003). The PtdIns(3,4,5)$P_3$-Akt-mTORC1 pathway is a major driver of cell growth and proliferation (Dey et al., 2017; Dibble and Manning, 2013; Manning and Toker, 2017; Sugiyama et al., 2019). As a result, mutations that hyperactivate this pathway are often associated with human cancers like triple-negative breast cancer (TNBC) (Dey et al., 2017; Li et al., 2017).

Given all this, we postulated that LCLAT1 disruption would impair EGF-mediated increase in PtdIns(3,4,5)$P_3$ levels and activation of downstream targets like Akt. In fact, we found that LCLAT1 silencing in at least two cell lines impeded EGF-mediated PtdIns(3,4,5)$P_3$ increase and Akt activation. This significantly impeded cell proliferation and survival, positioning LCLAT1 as a potential target for therapeutic drug development.

## Methods and Materials

### Cell Culture

The male human-derived ARPE-19 retinal pigment epithelial cell line was obtained from ATCC (CRL-2302, Manassas, VA) and was cultured in DMEM/F12 medium (ThermoFisher Scientific, Mississauga, ON) supplemented with 10% fetal bovine serum (Wisent, St. Bruno, QB), 100 U/mL penicillin and 100 µg/mL streptomycin (ThermoFisher Scientific). The female human-derived MDA-MB-231 triple negative breast cancer cell line was obtained from ATCC (CRM-HTB-26). Wild-type MDA-MB-231 cells and its derivatives (see below) were cultured in DMEM medium (Wisent) supplemented with 10% fetal bovine serum, 100 U/mL penicillin and 100 µg/mL streptomycin. The female human-derived HEK293T cell line was cultured in DMEM

with 10% fetal calf serum and 1% penicillin/streptomycin. All cells were cultured at 37°C and 5% $CO_2$.

**Transfection and siRNA-mediated gene silencing**

To silence gene expression of LCLAT1 in both ARPE-19 and MDA-MB-231 cells, custom-synthesized siRNA oligonucleotides against LCLAT1 were designed using Horizon Discovery siDESIGN Centre. We designed and tested siLCLAT1-1, siLCLAT1-7, and siLCLAT1-8 with the respective sequences 5'-GGAAAUGGAAGGAUGACAAUU-3', 5'CAGCAAGUCUCGAAGUAAUU-3', and 5'-UCGAAGACAUGAUUGAUUAUU-3'. Synthesis was by Sigma-Aldrich (Oakville, ON). In addition, we used siLCLAT1-5, a siGenome-validated oligonucleotide from Horizon (cat. D-010307-01-0002). Moreover, a non-targeting control siRNA (NT siRNA, or siCON) with the sequence 5'-CGUACUGCUUGCGAUACGGUU-3' was used (Sigma-Aldrich). Cells were transfected with 22 pmol of siRNA oligonucleotides/well using Lipofectamine RNAiMAX (ThermoFisher Scientifc) in Opti-MEM reduced serum media (ThermoFisher Scientific) for 3 h at 37°C and 5% $CO_2$ as per manufacturer's instructions. After transfection, cells were washed and incubated with fresh growth medium. Two rounds of transfection were performed, 72 and 48 h before each experiment.

**Plasmids and transfections**

Plasmid encoding PH-Akt-GFP was a kind gift from the Balla lab, NIH (Addgene: #51465) and was previously described in (Várnai and Balla, 1998). PH-Akt-GFP plasmid was transfected into ARPE-19 and MDA-MB-231 cells using Lipofectamine 3000 as instructed by the manufacturer.

Other plasmids used in this work were used to generate MDA-MB-231 cells equipped for inducible deletion of LCLAT1 by CRISPR-Cas9. All plasmids were obtained from Addgene (Watertown, MA): pMD2.G (Addgene: #12259) and psPAX2(Addgene: #12260) were kind gifts from Dr. Didier Trono; we also sued lenti Cas9-blast (Addgene: #52962; (Sanjana et al., 2014)), lentiguide-Puro (Addgene: #52963; (Sanjana et al., 2014)), and PXPR_011 (Addgene: #59702; (Doench et al., 2014)). The plasmid pEZ-Tet-pLKO-hygro (Addgene plasmid 85972; (Frank et al., 2017)) was adapted to express sgRNAs, and is hereafter referred to as "pEZ-TET-pLKO-guide-hygro".

**Lentivirus Production**

9 x$10^6$ HEK293T cells were seeded on 15 cm plates 24 hours prior to transfection with 50 µg of lentiviral vector, 37.5 µg of psPAX2, and 15 µg of pMD2.G per plate using the Calcium Phosphate method. Viral media was harvested 48 hours post-transfection, cleared via centrifugation at 500 xg for 10 min and filtered prior to concentration by ultracentrifugation at 50,000 g for 2.5 hours.

**MDA-MB-231 Cas9 Generation**

MDA-MB-231 cells were infected with lentiCas9-blast virus in the presence of 8 µg/mL protamine sulfate in a 6-well plate. Forty-eight hours post-transduction, media were changed and transduced cells were selected with 13 µg/mL blasticidin for seven days. CRISPR-Cas9 genome editing capability of MDA-MB-231 cells was tested as follows using an EGFP ablation assay. MDA-MB-231 and MDA-MB-231 Cas9 cells were infected with pXPR_011 virus in the presence of 8 µg/mL protamine sulfate in a 6-well plate. Forty-eight hours post-transfection,

media were changed and transduced cells were selected with 4 µg/mL puromycin for 2 days. GFP fluorescence was measured by flow cytometry 5 days post selection. The pXPR_011 plasmid contains both EGFP and a gRNA sequence that targets *EGFP*, and the percentage of GFP loss compared to control was used as a measurement of Cas9 activity.

**Inducible gRNA Construction**

gRNAs (Scaffold and Spacer) were PCR amplified using AccuPrime Pfx SuperMix (template and primers listed below) and digested with EcoRI and NheI overnight at 37°C. The pEZ-tet-pLKO-gRNA-hygR vector was digested with EcoRI and NheI overnight at 37°C, treated with Antarctic Phosphatase at 37°C for 1 hour, and gel purified using the QIAquick Gel Extraction Kit. The digested PCR products were purified and ligated into the linearized vector using T4 DNA ligase following the manufacturer's instructions. Ligation products were transformed into DH5α, prepped with the QIAGEN DNA Maxi Kit, and verified by Sanger Sequencing.

PCR Template: lentiGuide-puro

gLacZ forward: gctagcCCCGAATCTCTATCGTGCGGgttttagagctagaaatagcaagt

gLCLAT1-1 forward: GGCCgctagcACAACCGCCTTGTGGCAACAgttttagagctagaaatagcaagt

gLCLAT1-2 forward: GGCCgctagcTCTGATTGAGGAATGTTGTGgttttagagctagaaatagcaagt

gLCLAT1-3 forward: GGCCgctagcTGTAAAAGTGATTATAACTGgttttagagctagaaatagcaagt

Universal Scaffold reverse: CCGAATTCtcaagatctagttacgccaagctt

**Inducible Cas9-mediated LCLAT1 Knockout**

MDA-MB-231 Cas9 cells were infected with pEZ-tet-pLKO-gLacZ-hygR or pEZ-tet-pLKO-gLCLAT1-hygR virus in the presence of 8 µg/mL protamine sulfate in a 6-well plate. Forty-eight

hours post-transfection, media was changed and transduced cells were selected with 500 µg/mL hygromycin for 10 days. Thereafter, expression of LCLAT1-sgRNAs were induced by treatment of cells with 1 µg/ml of doxycycline for at least 48 hours.

**EGF signaling and Western blotting**

Before lysate preparation, cells were incubated with 2 mL of serum free growth medium for 1 h. After serum starvation, cells were stimulated with 5 ng/mL EGF for 5 or 10 min or left unstimulated (basal). Following serum starvation and subsequent EGF stimulation, whole cell lysates were prepared in 200 µL 2x Laemmli Sample Buffer (0.5M Tris, pH 6.8, glycerol and 10% sodium dodecyl sulfate (SDS)) supplemented with a protease and phosphatase inhibitor cocktail (Complete 1x protease inhibitor (Sigma-Aldrich), 1 mM sodium orthovanadate, and 10 nM okadaic acid). Lysates were heated at 65°C for 15 min and passed through a 27-gauge needle 10 times. Finally, 10% ß-mercaptoethanol and 5% bromophenol blue were added to cell lysates.

Proteins were resolved by Tris-glycine SDS-PAGE and transferred on to a polyvinylidene difluoride (PVDF) membrane. The PVDF membrane was blocked for 1 h at room temperature in blocking buffer composed of 3% bovine serum albumin (BSA) in 1X final Tris-buffered saline-Tween (TBS-T; 20 nM Tris, 150 mM NaCl and 0.1% Tween-20). After blocking, membranes were washed 3 times with wash buffer and incubated with 1:1000 primary antibody overnight at 4°C. The next day, membranes were washed 3 times, for 5 min each, and then subjected to 1:1000 secondary antibody for 1 h at room temperature. After incubation with secondary antibody, membranes were washed 3 times, 5 min each, and imaged using the ChemiDoc Imaging System (BioRad). Membranes were exposed to Immobilon Crescendo Western HRP substrate (Millipore Sigma) for 30-60 s and chemiluminescent images were

acquired by the ChemiDoc System. Western blot signals were analyzed and quantified using the ImageLab 6.1 (BioRad). Band intensity was obtained by signal integration in an area corresponding to the appropriate band. This value was then normalized to the loading control signal. Phosphorylated protein levels were normalized to total protein levels, and if necessary, the loading control.

Primary antibodies raised in rabbit were anti-LCLAT1 (cat. 106759, GeneTex), anti-phospho-Akt (S473, cat. 9271), anti-phospho-Akt1 (S473, cat. 9018), anti-phospho-Akt2 (S474, cat. 8599), anti-Akt1 (cat. 2938), anti-phospho-EGFR (Y1068. Cat. 2234), anti-phospho-tuberin/TSC2 (T1462, cat. 3611), anti-tuberin/TSC2 (cat. 3612), anti- phospho-MDM2 (S166, cat. 3521), anti-MDM2 (cat. 86934), anti-phospho-GSK3ß (S9, cat. 9323), anti-clathrin (cat. 4796), and anti-GAPDH (cat. 2118) were all from Cell Signaling Technologies. Antibodies raised in mouse were anti-Akt (cat. 2920), anti-Akt2 (cat. 5239), anti-GSK3ß (cat. 9832), and anti- puromycin (cat. MABE343) and were all from Cell Signaling Technology. Goat anti-EGFR antibodies were from Santa Cruz Biotechnology (sc-03-G). Horseradish peroxidase (HRP)-linked secondary anti-rabbit, anti-mouse, and anti-goat IgG antibodies were from Cell Signaling Technology.

**Puromycylation Assays**

Following siRNA transfection, cells were treated with or without 10 µg/mL puromycin for 10 min. Non-transfected control cells were treated with 10 µM cycloheximide for 20 min to block mRNA translation. Both puromycin and cycloheximide were obtained from Millipore Sigma. Whole cell lysates were prepared as above and subjected to Western blot analysis to probe for puromycin levels. Anti-puromycin primary antibodies (cat. MABE343) was from Cell Signaling

Technology and was prepared in a 1:1000 dilution and incubated overnight at 4°C. After which, the blot was washed 3x with wash buffer and incubated with 1:1000 anti-mouse (Cell Signaling Technology) secondary antibodies as described above.

**Immunofluorescence**

To detect surface levels of EGFR in MDA-MB-231 and ARPE-19 cells, cells were blocked with 3% BSA in PBS supplemented with 1 mM $CaCl_2$ and $MgCl_2$ for 30 min on ice, followed by 1 h incubation with a 1:200 dilution of mouse anti-EGFR antibody collected in-house from the mAb108 hybridoma obtained from ATCC (Cabral-Dias et al., 2022). After washing with PBS, cells were fixed with 4% paraformaldehyde in PBS for 15 min and then quenched with 100 mM glycine in PBS for 10 min, followed by washing with PBS, and then fluorescent secondary mouse antibodies (Jackson ImmunoResearch Labs Inc., West Grove, PA) at a 1:500 dilution in 1% BSA in PBS for 1 h at room temperature. The coverslips were mounted using Dako fluorescence mounting medium (Agilent Technologies, Inc. Mississauga, ON, Canada).

**Microscopy**

Confocal and TIRF micrographs were obtained using a Quorum Diskovery spinning disc confocal system coupled to a TIRF module (Quorum Technologies, Inc., Guelph, ON). The microscope itself consisted of an inverted fluorescence microscope (DMi8; Leica) equipped with an Andor Zyla 4.2 Megapixel sCMOS camera (Oxford Instruments, Belfast, UK), a 63x oil immersion objective (1.4 NA), and standard excitation and emission filter sets and lasers were used for all fluorophores. The TIRF module used a 63x/NA1.49 objective with a 1.8x camera

relay (total magnification 108x). The microscope system was controlled by the MetaMorph acquisition software (Molecular Devices, LLC, San Jose, CA, USA).

For fixed cells, z-stacks of 10-30 images were acquired with an inter-planal distance of 0.6 µm distance. For live-cell imaging of Akt-PH-GFP dynamics using spinning disc confocal or TIRF microscopy, cells were maintained in DMEM free of phenol red or serum in a Chamlide microscope-mounted chamber at 37°C and 5% $CO_2$. For timelapse of Akt-PH-GFP in MDA-MB-231 cells, a baseline was obtained by acquiring images for 1 min at 15 s, then EGF added and images acquired every 15 s for 10 min.

**Image Analysis and Processing**

Image processing and quantitative analysis were performed using ImageJ or FIJI v. 2.3 (Schindelin et al., 2012) or Volocity v. 7 (Quorum Technologies), where image enhancements were completed without altering the quantitative relationship between image elements. For quantification of EGFR cell surface, regions of interest were generated by freehand to define the cell outline, the mean fluorescence intensity over the whole cell area was calculated, and then background corrected (Cabral-Dias et al., 2022). Mean fluorescence from at least 30 cells per condition per experiment was then normalized against control condition. To obtain the relative cell surface localization index for the Akt-PH-GFP probe in ARPE-19 cells, we used ImageJ to determine the ratio of TIRF/epifluorescence fluorescence for >100 cells per condition per experiment. To measure the plasma membrane to cytosolic ratio of Akt-PH-GFP in MDA-MB-231 cells (Cabral-Dias et al., 2021), we used randomly selected regions of the plasma membrane and cytosol for each cell over timelapse movies using ImageJ and then calculated the fluorescence ratio. We examined 23 cells over three experiments.

**Cell Proliferation**

Cellular viability and cytotoxicity were measured using an Incucyte SX5 Live-Cell Analysis System (Sartorius). Cell death was assessed using CellTox Green Cytotoxicity Assay reagent (Promega G8741) at 1x final dilution in 12 mL of media and added to cells prior to imaging. Images were acquired at 30-min intervals for 72 h under 10x magnification using brightfield phase contrast and 300 ms exposure of 460 nm excitation, 524 nm emission to detect green fluorescence. Time-lapse image series were analyzed using the Incucyte Basic Analysis Software. Cellular confluence was normalized to initial phase contrast confluence for each sample.

**Lipid extraction**

Cells were grown to ~$0.5 \times 10^6$ per well in a 6-well plate. Cells were then placed on ice and the media removed. Cells were scraped in 500 μL of ice cold 1M HCl and transferred to a pre-cooled safe lock 2 mL microcentrifuge tube. Cells were then collected by centrifugation at 13,000 xg for 10 min at 4°C. The supernatant was aspirated, and the pellet was then snap frozen in liquid nitrogen.

**Mass Spectrometry Lipid Analysis**

Mass spectrometry was used to measure PtdInsPs from lipid extracts prepared from $0.5\text{-}1 \times 10^6$ MDA-MB-231 cells or $0.6 \times 10^6$ ARPE-19 cells as previously described (Clark et al., 2011). Briefly, we used a QTRAP 4000 mass spectrometer (AB Sciex, Macclesfield, UK) and employing the lipid extraction and derivatization method described for cultured cells (Clark et al., 2011). The response ratios of a specific PtdInsP acyl species were calculated by normalizing

the targeted lipid integrated response area to that of a known amount of added relevant internal standard. A ratio of ratios was then calculated by taking the response ratios of 38:4-PtdIns, 38-4-mono-PtdInsP, 38-4-bis-PtdInsP, and 38:4-PtdIns(3,4,5)$P_3$ against the sum of response ratios for 36:1 and 36:2 (36:x) of PtdIns or the corresponding 36:x-mono-PtdInsP or 36:x-bis-PtdInsP. Data are presented as mean ± STD from four separate experiments.

**Statistical analysis**

All experiments were repeated a minimum of three independent times, where specific repeats for each experiment are indicated in the respective figure legends. Data was collected as mean ± standard deviation (STD) or ± standard error of the mean (SEM) as appropriate. Statistical comparisons of means were then performed with GraphPad Prism v. 10. Statistical tests were elected by GraphPad based on the data conditions including number of conditions, sample size, and normality. Figure legends specify the tests employed for a given data set such as Student's t-test, one-way or two-way ANOVA tests, and associated post-hoc tests. P values are indicated in Figures, but a $p < 0.05$ was used to determine statistical significance.

## Results

**LCLAT1 acyltransferase regulation of EGFR trafficking**

In our previous work, LCLAT1 silencing altered the endocytosis and endosomal trafficking of the transferrin receptor in ARPE-19 cells (Bone et al., 2017). We thus queried if LCLAT1 disruption would alter the total and surface levels of EGFR and/or affect EGFR signalling in at least two human-derived cells lines: the non-transformed, male-derived ARPE-19 and the female-derived triple negative breast cancer cell line, MDA-MB-231. To do this, we used

previously designed and validated siRNA oligonucleotides against LCLAT1 (Bone et al., 2017) and a non-targeting oligonucleotide (see Methods), transiently transfected cells twice, and after 48 h, we lysed the cells and probed for LCLAT1 levels by Western blotting. As shown in Figure 1A and Figure 2A, respectively, control ARPE-19 and MDA-MB-231 cells displayed a major band at 35 kDa. After transfection with siLCLAT1-1, this band was reduced by >70% intensity in both cell types, manifesting efficient LCLAT1 silencing (Fig. 1A, B and Fig. 2A, B). We also observed reduced LCLAT1 expression in ARPE-19 and MDA-MB-231 cells transfected with independent siRNA oligonucleotides against LCLAT1 (Supplemental Figure S1A, B and S2A, B).

We next examined the effects of LCLAT1 silencing on total and surface levels of EGFR in these cells. We observed that LCLAT1 silencing in ARPE-19 cells did not alter total EGFR levels as measured by Western blotting (Fig. 1C, D) nor the EGFR surface levels as measured by immunofluorescence of unpermeabilized cells under basal conditions (Fig. 1E). The ability to internalize EGFR was also comparable between non-targeting and LCLAT1-silenced ARPE-19 cells as measured by a reduction in EGFR cell surface levels 1 h after supraphysiological 100 ng/mL EGF exposure (Fig. 1E). Importantly, LCLAT1-silencing did not impair EGF-mediated phosphorylation of Y1068 of EGFR – instead this was enhanced in LCLAT1-silenced cells (Fig. 1C, F). Overall, these data suggest that the steady-state levels and trafficking of EGFR, and immediate response to EGF in ARPE-19 cells were not affected by LCLAT1 silencing.

We subsequently tested LCLAT1-silencing on MDA-MB-231 cells. As with ARPE-19 cells, suppressing LCLAT1 cells in MDA-MB-231 cells did not significantly alter total levels of EGFR relative to control cells as measured by Western blotting (Fig. 2C, D). Moreover, control and LCLAT1-silenced cells displayed similar levels of surface EGFR under basal conditions,

which dropped by similar levels after EGF stimulation (Fig. 2E). As with ARPE-19 cells, EGF boosted the phosphorylation of Y1068-EGFR in control and LCLAT1-silenced MDA-MB-231 cells relative to serum-starved cells (Fig. 2F). Finally, we measured turnover of EGFR upon EGFR in MDA-MB-231 cells. Controls cells accumulated EGFR upon 90 min of high-levels of EGF stimulation (Fig. 2G, H). However, LCLAT1-silenced MDA-MB-231 cells did not accumulate EGFR upon the same treatment, indicating that LCLAT1 activity is required for EGFR stability in this context (Fig. 2G, H). Thus, while MDA-MB-231 cells had similar total and surface levels of EGFR under basal conditions and could respond to EGF, EGFR stability post-signaling was altered upon loss of LCLAT1 expression.

**LCLAT1 acyltransferase silencing reduces PtdIns(3,4,5)$P_3$ synthesis in response to EGF**

A key outcome of EGFR stimulation is the synthesis of PtdIns(3,4,5)$P_3$ and/or PtdIns(3,4)$P_2$ levels by activating the PI3Ks (Hu et al., 1992; Orofiamma et al., 2022; Rodrigues et al., 2000). To assess this, we transfected ARPE-19 and MDA-MB-231 cells with Akt-PH-GFP, a biosensor for 3-phosphorylated PtdInsPs (Várnai and Balla, 1998). The recruitment of Akt-PH-GFP to the plasma membrane in response to EGF was then quantified using two different methods. Given that ARPE-19 cells are exceptionally flat, we quantified the ratio of TIRF to epifluorescence fields (TIRF/Epi fluorescence ratio) as an indicator for PtdIns(3,4,5)$P_3$ levels at the plasma membrane. By comparing EGF-stimulated non-targeted and LCLAT1-silenced cells, we observed a lower Akt-PH-GFP TIRF/Epi fluorescence ratio in latter cells, nearly comparable to cells incubated with the PI3K inhibitor, LY294002 (Fig. 3A, B). Thus, despite normal EGFR levels and early response, ARPE-19 cells were defective in EGF-mediated PI3K signalling. We then assessed if MDA-MB-231 cells were also impaired for PI3K signalling. Since these cells are rounder, preventing a similar straightforward approach of monitoring the intensity of the Akt-

PH-GFP probe in the TIRF field, we measured Akt-PH-GFP on the plasma membrane more readily by sampling Akt-PH-GFP at the cell periphery against cytosolic signal. We tracked the Akt-PH-GFP recruitment over 10 min after adding EGF. Again, we observed an increase in Akt-PH-GFP to the cell periphery after EGF stimulation on non-silenced MDA-MB-231 cells (Fig. 3C, D). Importantly, this increase in Akt-PH-GFP at the cell periphery in response to EGF was significantly suppressed in the LCLAT1-silenced cell group (Fig. 3C, D). Hence, LCLAT1 expression is required to support EGF-EGFR lipid signalling in these cells.

**The impact of LCLAT1 acyltransferase expression on the acyl profile of PtdInsPs**

We next determined the PtdInsP acyl profile and relative levels by mass spectrometry in control, serum starved, and EGF-stimulated non-silenced and LCLAT1-silenced ARPE-19 and MDA-MB-231 cells. For this analysis, we normalized lipid spectral counts against synthetic standards added to the samples to generate a response ratio (see methods). In addition, to correct for variation in cell input between experiments, we further normalized against an internal benchmark by comparing changes in 38:4 PtdIns, *mono*-PtdInsPs, *bis*-PtdInsPs, and PtdIns(3,4,5)$P_3$ relative to standardized 36:x-PtdIns and the corresponding 36:x-mono-PtdInsP and 36:xbis-PtdInsP since these species have previously been shown to be less affected by LCLAT1 expression relative to 38:4 species (Bone et al., 2017; Imae et al., 2012). We note that our previous normalization benchmark used the 38:x PtdInsP to its respective 36:x PtdInsP – for example, we compared 38:x-*bis*-PtdInsPs to 36:x-*bis*-PtdInsPs and internal benchmark was not used (Bone et al., 2017).

For ARPE-19 cells, the major acyl species of PtdIns, *mono*-, *bis*-, and *tris*-PtdInsP was 38:4, as expected. In fact, we only detected 38:4 acyl species for PtdIns(3,4,5)$P_3$. We then compared each group of 38:4 PtdInsPs to the 36:x-PtdIns and the corresponding 36:x-PtdInsP.

Relative to 36:x-PtdIns, we saw that the relative levels of 38:4-PtdIns was reduced in LCLAT1-silenced cells (Fig. 4A). In comparison, there was no significant difference in 38:4-*mono*-PtdInsPs relative to 36:x-PtdIns or 36:x-mono-PtdInsP in any treatment (Fig. 4B, Sup. Fig. S3A). In comparison, 38:4-*bis*-PtdInsPs was more likely to be lower in LCLAT1-silenced cells relative to both 36:x-PtdIns (Fig. 4C) and 36:x-bis-PtdInsPs (Sup. Fig. S3B) than control silenced cells. Lastly, EGF-stimulated LCLAT1-silenced cells had lower 38:4-PtdIns(3,4,5)$P_3$ levels relative to 36:x-PtdIns than non-targeted ARPE-19 cells (Fig. 4D). We could not quantitatively compare 38:4-PtdIns(3,4,5)$P_3$ to 36:x-PtdIns(3,4,5)$P_3$ since we did not detect the latter; but nonetheless, this suggests that 38:4-PtdIns(3,4,5)$P_3$ is the predominant acyl species of this phosphoinositide upon EGF stimulation. Overall, ARPE-19 cells appeared to shift in the acyl profile of PtdIns, bis-PtdInsPs, and PtdIns(3,4,5)P3 upon LCLAT1-disruption.

We similarly investigated the lipidomic profile of MDA-MB-231 cells. The major acyl species for all PtdInsPs and PtdIns was again 38:4 and we once again only detected 38:4-PtdIns(3,4,5)$P_3$ acyl species in our samples. Interestingly, and unlike ARPE-19 cells, LCLAT1 suppression did not alter the levels of 38:4-PtdIns, 38:4-*mono*-PtdInsPs or 38:4-*bis*-PtdInsPs relative to 36:x-PtdIns or the respective 36:x-mono-PtdInsP or 36:x-bis-PtdInsP whether cells were resting, serum-starved or EGF-stimulated (Figure 4E, F, G, Sup. Fig. S4C, D). The exception was a statistical difference that we measured for 38:4-mono-PtdInsP relative to 36:x-mono-PtdInsP in resting cells (Fig. S4C). Despite these observations, the relative levels of 38:4-PtdIns(3,4,5)$P_3$ were once again abated after EGF stimulation in LCLAT1-perturbed cells relative to 36:x-PtdIns (Fig. 4H). Overall, we propose that LCLAT1 expression is essential to support EGFR-dependent activation of PI3K signalling in at least two distinct cell lines, but the impact on acyl profile can vary between cell type, lipid benchmarks, and treatments.

**LCLAT1 acyltransferase silencing disrupts EGF-mediated Akt activation**

Since LCLAT1-silenced cells have lower EGF-induced PtdInsP(3,4,5)$P_3$ levels relative to non-silenced counterparts, we next examined if Akt activation was also impaired in ARPE-19 and MDA-MB-231 cells after EGF exposure. To do this, we probed for phosphorylation at S473 using an antibody that recognizes all isoforms of Akt when phosphorylated (pan-phospho-Akt antibody). Relative to serum-starved ARPE-19 and MDA-MB-231 cells, EGF caused a large increase in phospho-Akt in non-silenced control cells (Fig. 5A, B and Fig. 6A, B). Importantly, both ARPE-19 and MDA-MB-231 cells silenced for LCLAT1 displayed a substantial reduction in phospho-Akt after EGF stimulation (Fig. 5A, B and Fig. 6A, B). We also observed impaired p-Akt levels in ARPE-19 cells (Supplemental Figure S1A, C) and MDA-MB-231 cells (Supplemental Figure S2A, C) silenced for LCLAT1 using independent oligonucleotides against LCLAT1. To determine if this impairment was isoform specific, we then re-probed with anti-p-Akt1 (S473) and p-Akt2 (S474) antibodies. We observed lower levels of p-Akt1 relative to total Akt1 in both ARPE-19 and MDA-MB-231 silenced for LCLAT1 after EGF stimulation (Fig. 5C, D and Fig. 6C, D). In addition, LCLAT1 silencing potently impaired activation of Akt2 in both ARPE-19 and MDA-MB-231 cells (Fig. 5C-F and Fig. 6C-F). Thus, LCLAT1 silencing negatively and broadly impacts Akt activation.

**LCLAT1 acyltransferase silencing impairs Akt-mediated regulation of downstream targets**

Since Akt activation is defective in LCLAT1-silenced cells after addition of EGF, we next examined if this effect percolated to several known Akt targets. To test for specific targets, we measured the phosphorylation state of Tsc2, GSK3β, and Mdm2 using anti-p-TSC2 (T1462),

anti-p-GSK3ß (S9), and anti-p-MDM2 (S166). In ARPE-19 and MDA-MB-231 cells transfected with non-targeting oligonucleotides, EGF promoted phosphorylation of these specific Akt substrates (Fig. 7). By contrast, LCLAT1-silenced cells suffered a considerable reduction in this EGF-induced phosphorylation of Tsc2 and GSK3β normalized to their respective totals (Fig. 7A-D, 7G-J). Interestingly, while there was an apparent decrease in p-MDM2 after EGF stimulation in LCLAT1-silenced cells, when normalized to total MDM2, there was little difference (Fig. 7E, F, K, L). Instead, total MDM2 protein expression was significantly reduced in LCLAT1-sienced MDA-MB-231 cells indicating an additional regulatory level imposed on MDM2 that depends on LCLAT1 expression (Fig. 7E, F, K, L).

**LCLAT1 acyltransferase disruption impairs cell growth**

Our observations hereto suggest that LCLAT1 expression supports the PtdIns(3,4,5)$P_3$-Akt signalling pathway in response to EGF signaling. This pathway is essential to promote cell proliferation and survival. We thus predicted that loss of LCLAT1 expression would impede cell proliferation and/or survival. For these experiments, we first focused on MDA-MB-231 cells transiently silenced for LCLAT1. We tracked growth of LCLAT1-silenced and control MDA-MB-231 cells in an Incucyte system and quantified change in confluency as a measure of growth (Supplemental Videos 1 and 2). Concurrently, we tracked cell death by staining with CellTox Green and quantifying number of stained dead cells (Supplemental Videos 1 and 2). As shown in Fig. 8A-C and Supplemental Videos, we found that MDA-MB-231 cells stagnated in their growth and died at a greater rate than cells exposed to non-targeting siRNA oligonucleotides. However, since these observations require prolonged observation, we complemented transient gene silencing with a model that allows for inducible, yet stable disruption of LCLAT1

expression. We generated MDA-MB-231 cells that constitutively expressed the Cas9 recombinase (Supplemental Figure S4A). These cells were then further modified by the stable insertion of doxycycline-inducible expression of gRNAs targeting LCLAT. We generated three cell lines using three different gRNAs and tested the efficiency of induced CRISPR-based knockout of LCLAT1 in these MDA-MB-231-Cas9 sublines by treating cells with 0.1 or 1 µg/mL doxycycline over 3-5 days and then probed for LCLAT1 expression. We found that gRNA2 was most efficient at disrupting LCLAT1 expression (Sup. Fig. S4B, C). Importantly, MDA-MB-231::Cas9 expressing gRNA2 against LCLAT1 also possessed lower phospho-Akt levels under basal growth conditions (Sup. Fig. S4D-F).

Having established this new model system to investigate the role of LCLAT1 in MDA-MB-231 cells, we next assessed the ability of these cells to proliferate and survive after LCLAT1 deletion. To do this, we used the Incucyte SX5 imaging incubator system over 72 h and tracked change in confluency as an indicator or proliferation. As shown in Fig. 8D, E and Supplemental Videos 3 and 4, MDA-MB-231-Cas9 cells became confluent over 72 h with or without doxycycline. In comparison, MDA-MB-231-Cas9 cells engineered with the LCLAT1 gRNA2 and exposed to doxycycline to delete LCLAT1 grew at a slower rate relative to its counterparts without doxycycline and parent MDA-MB-231-Cas9 cells (Fig. 8D, E, Sup. Videos 5 and 6). This lower cell growth was consistent with reduced protein synthesis upon LCLAT1 silencing observed using puromycylation assays (Fig. 8F, G). Overall, LCLAT1 expression is needed to support EGF signalling and its PtdIns(3,4,5)$P_3$-Akt pathway in at least two distinct cell types and to promote cell proliferation and survival.

## Discussion

Here, we reveal that the LCLAT1 acyltransferase supports EGFR-mediated PtdIns(3,4,5)$P_3$-Akt signaling to promote cell proliferation in at least two cell lines. While MDA-MB-231 and ARPE-19 cells displayed some minor differences in the effects of LCLAT1 silencing, we showed here that LCLAT1 is needed to increase PtdIns(3,4,5)$P_3$ levels during EGF stimulation. Consequently, LCLAT1-silenced cells were impaired for Akt activation, phosphorylation of Akt substrates, and ultimately, they were impaired for proliferation. We thus identified an important role for the poorly studied LCLAT1 acyltransferase in PI3K-Akt signalling downstream of EGF-EGFR engagement.

*The role of LCLAT1 in generating PtdIns(3,4,5)$P_3$*

We provide at least three pieces of evidence that LCLAT1 is important to generate PtdIns(3,4,5)$P_3$ during EGF-mediated signalling. First, we revealed that LCLAT1-silenced MDA-MB-231 and ARPE-19 cells were impaired for the recruitment of the Akt-PH-GFP, a biosensor for PtdIns(3,4,5)$P_3$ levels (Haugh et al., 2000; Marshall et al., 2001), to the plasma membrane after EGF stimulation. Second, we observed that LCLAT1-silenced cells possessed lower relative levels of 38:4-PtdIns(3,4,5)$P_3$. Incidentally, 38:4-PtdIns(3,4,5)$P_3$ was the only observable acyl-based species for PtdIns(3,4,5)$P_3$ in both cell types, likely because the other acyl isoforms of PtdIns(3,4,5)$P_3$ were below the detection limit of our current analysis. Regardless, this is consistent with other studies examining the acyl profile of PtdIns(3,4,5)$P_3$, identifying 38:4 as the major species of this PtdInsP, though this can vary with tissue, cell type, and genetics (Clark et al., 2011; Koizumi et al., 2019; Morioka et al., 2022; Mujalli et al., 2018). Third, Akt activation was impaired in LCLAT1-silenced cells after EGF stimulation. Hence, collectively

these varied approaches indicate that LCLAT1-silenced cells are defective in promoting PtdIns(3,4,5)$P_3$ levels, and possibly PtdIns(3,4)$P_2$.

A key question then is how does LCLAT1 contribute to PtdIns(3,4,5)$P_3$ synthesis. We propose at least three possible, non-mutually exclusive mechanisms that will need to be defined in future studies. First, enzymes involved in PtdIns(3,4,5)$P_3$ metabolism such as Class I PI3Ks, the PTEN 3-phosphatase, and SHIP1/2 5-phosphatase may display acyl sensitivity towards their substrates as previously suggested (Anderson et al., 2016), thus affecting PtdIns(3,4,5)$P_3$ generation or its turnover. This was observed for Type I PIPKs, Vps34 Class III PI3Ks, and Type II phosphatases (Ohashi et al., 2020; Schmid et al., 2004; Shulga et al., 2012). Second, PtdIns(3,4,5)$P_3$ may be reduced in LCLAT1-disturbed cells due to lower PtdIns(4,5)$P_2$ substrate levels or availability. For example, we previously demonstrated in ARPE-19 cells that LCLAT1 silencing lowered the total levels of PtdIns(4,5)$P_2$ and altered its subcellular distribution (Bone et al., 2017). Third, and perhaps linked to the second model above, PtdIns(3,4,5)$P_3$ synthesis may depend on specific substrate pools. These pools may be highly localized or even channeled through scaffolds (Choi et al., 2016) or transferred at membrane contact sites (Zaman et al., 2020). For example, depletion of bulk PtdIns(4)P from the plasma membrane did not impact PtdIns(4,5)$P_2$ levels (Hammond et al., 2012), possibly because PtdIns(4,5)$P_2$ depends on specific pools of PtdIns(4)P. Moreover, contact sites between endoplasmic reticulum and the plasma membrane are important to generate PtdIns and PtdIns(4,5)$P_2$ (Chang and Liou, 2015; Cockcroft et al., 2016; Kim et al., 2015; Lees et al., 2017; Saheki et al., 2016; Zaman et al., 2020). Thus, LCLAT1 may play a role in generating specific substrate pools to support PtdIns(4,5)$P_2$ and PtdIns(3,4,5)$P_3$ at the plasma membrane.

The idea that LCLAT1 may act on specific pools of PtdInsPs is consistent with observations that LCLAT1 and LPIAT/MBOAT7 do not affect the levels of and the acyl profile of all PtdInsPs. For example, their disruption preferentially affects the acyl profile of PtdIns and/or *bis*-phosphorylated PtdInsPs, but not mono-PtdInsPs (Anderson et al., 2013; Bone et al., 2017) and in this work. Moreover, other than PtdIns(3,4,5)$P_3$, we were surprised to see that LCLAT1 expression did not impact PtdInsPs in MDA-MB-231 cells – this may be because LCLAT1 acts on highly specialized pools of lipids in these cells and/or that other acyltransferases are at play. Overall, while we know that LCLAT1 supports cells to boost PtdIns(3,4,5)$P_3$ levels in response to EGF, the exact mechanism of action remains to be defined.

*LCLAT1 and PtdIns(3,4,5)$P_3$ functions*

We witnessed that LCLAT1 supports PtdIns(3,4,5)$P_3$-mediated activation of Akt isoforms after EGF signalling. Consequently, targets of Akt such as TSC2 and GSK3β, displayed reduced phosphorylation in LCLAT1-silenced cells, while Mdm2 stability was affected by LCLAT1 silencing. Hence, we anticipate that LCLAT1 also supports other effector functions of PtdIns(3,4,5)$P_3$ including activation of other kinases such as Btk (Bolland et al., 1998; Lien et al., 2017) and GEFs for the Rho-family of GTPases such as Vav1 and Tiam1 (Salamon and Backer, 2013; Wang et al., 2006, 2; Zhu et al., 2015, 1). Additionally, while our work focused on EGFR-mediated signalling, we postulate that LCLAT1 also supports signalling by other receptor tyrosine kinases such as the Met receptor, FGF, and insulin-like growth factor receptor, and may also support signalling by GPCRs and kinase-associated receptors such as immune receptors (Bresnick and Backer, 2019; Dowling and Mansell, 2016; Getahun and Cambier, 2015; Takeuchi and Ito, 2011). Conceivably, the putative role of LCLAT1 in promoting PI3K

signalling among these receptor classes may depend on which isoforms of Class I and/or Class II PI3K are engaged (Bilanges et al., 2019; Duncan et al., 2020). Overall, our observations establish a key relationship between LCLAT1 and EGFR-PtdIns(3,4,5)$P_3$-Akt axis and sets a course to determine the universality of LCLAT1 acyltransferase in PtdIns(3,4,5)$P_3$ signalling.

*LCLAT1 in cellular function and therapeutic potential*

While the LCLAT1 acyltransferase remains relatively under-investigated, LCLAT1 is associated with hematopoiesis and cell differentiation (Huang et al., 2014; Huang et al., 2017; Wang et al., 2007; Xiong et al., 2008), metabolic regulation (Cao et al., 2009, 1; Liu et al., 2012, 1), mitochondrial stability, dynamics and function (Huang et al., 2020; Li et al., 2010, 1; Li et al., 2012, 1), sensitivity to oxidative stress (Li et al., 2010; Liu et al., 2012, 1), endocytosis and endosomal trafficking (Bone et al., 2017), and now EGFR signalling. LCLAT1 is also proposed to remodel the acyl profile of both cardiolipin and PtdIns/PtdInsPs (Bone et al., 2017; Cao et al., 2004, 1; Imae et al., 2012; Li et al., 2010, 1). It is generally thought that mitochondrial and oxidative stress occurs through cardiolipin remodelling, while endocytosis and receptor signalling is connected to PtdIns acyl function, as proposed here. However, the specific roles of LCLAT1 in cardiolipin and PtdInsP acyl remodelling have not been reconciled. It may be that LCLAT1 has independent roles in acylating these two distinct lipids, or alternatively, one may depend on the other. For example, mitochondria contain PtdIns on their outer membrane, which is important for mitochondria dynamics and function (Pemberton et al., 2020; Zewe et al., 2020). Conceivably, then LCLAT1 acylation of PtdIns may impact lipidomic properties of cardiolipin in mitochondria. Regardless, LCLAT1 and its putative partner, MBOAT7/LPIAT1, remain relatively understudied and without known inhibitors. Given the role of LCLAT1 in PtdInsP

biology and receptor signalling, we propose that these acyltransferases represent new targets for therapeutic development to complement existing PI3K and Akt inhibitors.

Overall, our work shows that LCLAT1 acyltransferase supports receptor tyrosine kinase signalling by enabling PtdIns(3,4,5)$P_3$ synthesis and Akt signalling, supporting cell survival and proliferation. While the exact mechanism of action is not known, our work positions LCLAT1 and acyltransferases such as MBOAT7/LPIAT1 for further study and as potential drug targets against conditions like cancer that depend on PtdIns(3,4,5)$P_3$ signalling.

**Figure legends**

**Figure 1: LCLAT1 silencing has no negative impact on EGFR activation, EGFR total levels, and EGFR surface levels in ARPE-19 cells. A.** Western blotting showing repressed LCLAT1 expression in ARPE-19 cells transfected with siLCLAT1-1 oligonucleotides relative to cells exposed to a non-targeting control siRNA (NT siRNA). C = control or standard media; SS = Serum-starved; EGF = EGF for 5 min. Clathrin heavy chain (CHC) was used as a loading control. **B.** Quantification of LCLAT1 silencing by normalizing LCLAT1 signal to CHC in ARPE-19 cells. **C.** ARPE-19 cells silenced for LCLAT1 or treated with non-targeting oligonucleotide were serum-starved and then stimulated with EGF for 5 min. Lysates were then probed for total EGFR or phospho-EGFR. GAPDH was employed as the loading control. **D.** Quantification of total EGFR relative to the respective GAPDH signal. **E.** Normalized cell surface EGFR detected by immunofluorescence before and after 1 h EGF stimulation in non-targeted and LCLAT1-silenced ARPE-19 cells. **F.** Quantification of phosphor-EGFR (p-Y1068)

relative to the respective EGFR signal. All experiments were repeated a minimum of three times. For B, D, and F shown is mean ±STD. Data in E is shown as mean ± SEM where at least 40-80 cells were scored per condition per experiment. Data in B and D were analysed by an unpaired Mann-Whitney test. For data in E and F, a two-way ANOVA followed by Sidak's post-hoc test was used. * represents $p<0.05$, ** represents $p<0.01$.

**Figure 2: LCLAT1 silencing has minor impact on EGFR activation, total EGFR levels, and surface EGFR levels, but affects EGFR stability in MDA-MB-231 cells. A.** Western blotting showing LCLAT1 silencing in MDA-MB-231 cells transfected with siLCLAT1-1 (siLC-1) relative to cells exposed to non-targeting control siRNA (NT siRNA). SS = Serum-starved; EGF = EGF for 5 min. Clathrin heavy chain (CHC) was used as a loading control. **B.** Quantification of LCLAT1 silencing by normalizing LCLAT1 to CHC signal. **C.** MDA-MB-231 cells silenced for LCLAT1 or treated with non-targeting oligonucleotides were serum-starved and then stimulated with EGF for 5 min. Lysates were then probed for total EGFR or phospho-EGFR (pY-1068). GAPDH was employed as the loading control. **D.** Quantification of total EGFR relative to respective GAPDH. **E.** Normalized cell surface EGFR detected by immunofluorescence before and after 1 h EGF stimulation in non-targeted and LCLAT1-silenced MDA-MB-231 cells. **F.** Quantification of phospho-Y1068-EGFR relative to EGFR. **G.** MDA-MB-231 cells mock-silenced or LCLAT1-silenced were serum-starved and concurrently incubated with 100 ng/mL EGF and cycloheximide for the indicated times. Lysates were then probed for total EGFR and GAPDH. **H.** Quantification of EGFR stability during high EGF stimulation of MDA-MB-231 cells treated with cycloheximide. EGFR was first normalized to corresponding GAPDH. Values were then further normalized to the corresponding time zero of

control and LCLAT1-silenced cells. All experiments were repeated three independent times. For B, D, F, and H, shown are the mean ±STD. For E, the mean ±SEM is shown where 50-100 cells were scored per condition per experiment. Data in B and D was tested by an unpaired Mann Whitney test. For data in E, F, and H, a two-way ANOVA and Sidak's post-hoc test were used. *, **, and *** respectively represent $p<0.05$, $p<0.01$, and $p<0.001$.

**Figure 3. LCLAT1 expression supports EGF-stimulated PtdIns(3,4,5)$P_3$ synthesis.** ARPE-19 (A) and MDA-MB-231 cells (C) were mock-silenced or LCLAT1-silenced and then transfected with plasmid DNA expressing Akt-PH-GFP, followed by serum-starvation and stimulation with EGF. **A.** TIRF and epifluorescence microscopy of ARPE-19 cells 5 min after EGF stimulation. **B.** Quantification of TIRF/epifluorescence ratio of Akt-PH-GFP. Total Akt-PH-GFP fluorescence in TIRF field is expressed as a ratio against the corresponding total fluorescence in the epifluorescence field. Mock-silenced and LCLAT1-silenced cells were treated with EGF. As a positive control for this approach, we pre-treated cells with the PI3K inhibitor, LY294002, which ablated Akt-PH-GFP recruitment to the TIRF field. **C.** Spinning disc confocal images of MDA-MB-231 cells mock-silenced or LCLAT1-silenced before and EGF stimulation. **D.** Quantification of Akt-PH-GFP fluorescence at the plasma membrane relative to its cytosolic signal from time-lapse imaging over 10 min of EGF stimulation. Scale bar = 20 µm. All experiments were repeated three independent times. Shown is the mean ±SEM, where data in D was binned every 45 sec (three images). For B, data is based on 30-50 transfected cells per condition per experiment. For D, a total of 23 transfected cells were traced over time. A one-way

ANOVA and Sidak's post-hoc test was used to test data in B and D. * and *** respectively represent $p<0.05$ and $p<0.001$.

**Figure 4. Relative levels of 38:4 PtdIns and PtdInPs in ARPE-19 and MDA-MB-231 cells silenced for LCLAT1.** ARPE-19 cells (**A-D**) and MBA-MB-231 cells (**E-I**) were mock silenced (siCon) or LCLAT1-silenced. Cells were then grown in regular medium (control), serum-starved (ss), and stimulated with EGF for 5 min (EGF). Reactions were quenched and lipid extracted after addition of internal standards to primary cell extracts. PtdInsPs were measured by mass spectrometry (HPLC-MS). Shown is the ratio of standardized 38:4-PtdIns (A, E), 38:4-mono-PtdInsP (B, G), 38:4-bis-PtdInsP (C, H), and 38:4-PtdIns(3,4,5)$P_3$ (D, I) to the standardized sum of 36:1 and 36:2-PtdIns (referred to as 36:x-PtdIns). Lipid analysis was repeated four independent times. Shown are the mean ±STD. A two-way ANOVA and Sidak's post-hoc test was used to test data, where * and ** respectively represent $p<0.05$ and $p<0.01$.

**Figure 5: LCLAT1 is required for EGF-stimulated Akt activation in ARPE-19 cells**. **A, C, E:** Mock-silenced and LCLAT1-silenced ARPE-19 cells were serum-starved (0 min) or stimulated with EGF for 5 min. Lysates were then prepared, separated by SDS-PAGE and probed by Western blotting for pan-phospho-Akt and total pan-Akt (A), phospho-Akt1 and total Akt1 (C), and phospho-Akt2 and total Akt2 (E). Clathrin heavy chain (CHC) or GAPDH were used as loading controls. **B, D, F**: Quantification of pan-pAkt (B), pAkt1 (D), and pAkt2 (F) normalized to respective total pan-Akt, Akt1, and Akt2. Mean ±STD are shown from n=3 independent experiments are shown. A two-way ANOVA and Sidak's post-hoc test was used to statistically test the data, where * represents $p<0.05$.

**Figure 6: LCLAT1 is required for EGF-stimulated Akt activation in MDA-MB-231 cells**. **A, C, E:** Mock-silenced and LCLAT1-silenced MDA-MB-231 cells were serum-starved (0 min) or stimulated with EGF for 5 min or 10 min. Lysates were then prepared, separated by SDS-PAGE and probed by Western blotting for pan-phospho-Akt and total pan-Akt (A), phospho-Akt1 and total Akt1 (C), and phospho-Akt2 and total Akt2 (E). Clathrin heavy chain (CHC) or GAPDH were used as loading controls. **B, D, F**: Quantification of pan-pAkt (B), pAkt1 (D), and pAkt2 (F) normalized to respective total pan-Akt, Akt1, and Akt2. Mean ±STD are shown from n=3 independent experiments are shown. A two-way ANOVA and Sidak's post-hoc test was used to statistically test the data, where *, **, and **** respectively represent $p<0.05$, $p<0.01$, and $p<0.0001$.

**Figure 7: LCLAT1 is required for activation of Akt substrates after EGF stimulation**. **A, C, E:** Mock-silenced and LCLAT1-silenced ARPE-19 cells were serum-starved (0 min) or stimulated with EGF for 5 min. Lysates were then separated by SDS-PAGE and probed by Western blotting for phospho-Tsc2 and total Tsc2 (A), phospho-GSK3β and total GSK3β (C), and phospho-Mdm2 and total Mdm2 (E). Clathrin heavy chain (CHC) or GAPDH were used as loading controls. **B, D, F**: Quantification of pTsc2 (B), pGSK3β (D), and pMdm2 (F) normalized to respective total Tsc2, GSK3β, and Mdm2. **G, I, K**: Mock-silenced and LCLAT1-silenced MDA-MB-231 cells were serum-starved (0 min) or stimulated with EGF for 5 min. Lysates were then separated by SDS-PAGE and probed by Western blotting for phospho-Tsc2 and total Tsc2 (G), phospho-GSK3β and total GSK3β (I), and phospho-Mdm2 and total Mdm2 (K). Clathrin heavy chain (CHC) or GAPDH were used as loading controls. **H, J, L**: Quantification of pTsc2

(H), pGSK3β (I), and pMdm2 (K) normalized to respective total Tsc2, GSK3β, and Mdm2. For G, I, K, H, J, and L, mean ±STD are shown from n=3 independent experiments. A two-way ANOVA and Sidak's post-hoc test was used to statistically test the data, where * represents $p<0.05$.

**Figure 8: LCLAT1 is required for cell growth and/or survival. A.** Frames at indicated time points of mock and LCLAT1-silenced MDA-MB-231 cells over 72 h using Incucyte. Cells were stained with CytoTox Green to track cell death. Images were acquired from Supplemental Videos X and Y. **B.** Quantification of cell confluency over 72 h. **C**. Quantification of cell death (CytoTox Green objects) over 72 h. **D.** Frames at indicated time points of cells expressing Cas9 and non-targeted gRNA (top panels) or Cas9-gRNA against LCLAT1 (bottom panels). Non-targeted and gRNA-LCLAT1 expression were either not expressed (no doxycycline) or induced by adding doxycycline. Cells were exposed to CytoTox Green to track cell death. **E.** Quantification of cell confluency of CRISPR-engineered MDA-MB-231 cells as shown in D. B, C, and E. Shown is the mean ± STD of three independent experiments. Last data point was analysed by two-way ANOVA and Tukey's post-hoc test. * represents $p<0.05$. **F.** MDA-MB-231 cells were transfected with non-targeting siRNA (NT siRNA) or siLCLAT1-1. Cells were then exposed to vehicle or cycloheximide (CHX), followed by puromycin to label proteins during translation. Cells were prepared and probed with anti-puromcyin antibodies to detect puromycylated proteins. Clathrin was use as a loading control. **G.** The relative puromycin signal in each lane as shown in F was quantified relative to clathrin signal. Shown is the mean ± STD of three independent experiments, analysed by one-way ANOVA and Tukey's test. * represents $p<0.05$.

## Supplemental Information

**Supplemental Figure S1: LCLAT1 silencing in ARPE-19 cells with an independent siRNA oligonucleotide disrupts Akt signalling.** ARPE-19 cells were transfected with oligonucleotide siLCLAT1-5 or non-targeting control. Cells were then serum-starved (SS), followed by EGF stimulation for 5 min. **A.** Lysates were probed for LCLAT1 expression, p-Akt, Akt, and clathrin heavy chain (CHC), which was used as a loading control. **B.** Quantification of LCLAT1 silencing by normalizing LCLAT1 to CHC signal in ARPE-19 cells. **C.** Quantification of p-Akt levels relative to total Akt. Data is shown as mean ±STD are shown from n=3 independent experiments. Data was analysed by a one-way ANOVA and Sidak's post-hoc test, where *, **, ***, and respectively represent $p<0.05$, $p<0.01$, $p<0.001$, and $p<0.0001$, respectively.

**Supplemental Figure S2: LCLAT1 silencing in MDA-MB-231 cells with independent siRNA oligonucleotides disrupts Akt signalling.** **A.** Western blotting showing LCLAT1 silencing in MDA-MB-231 cells transfected with non-targeting siRNA, siLCLAT1-1, siLCLAT1-7, or siLCLAT1-8 oligonucleotides. Cells were then serum-starved (SS) or stimulated with EGF for 5 min. Lysates were probed for LCLAT1 expression, p-Akt, and clathrin heavy chain (CHC), which was used as a loading control. **B.** Quantification of LCLAT1 silencing by normalizing LCLAT1 to CHC signal in MDA-MB-231 cells transfected as in D. **C.** Quantification of p-Akt levels relative to clathrin in MDA-MB-231 cells mock-silenced or LCLAT1-silenced with one of three siRNA oligonucleotides and either serum-starved or

stimulated with EGF for 5 min. Show is the mean ±STD from n=3 independent experiments. Data in B was analysed with a one-way ANOVA and Dunnett's post-hoc test. Data in C was analysed with a two-way ANOVA and Sidak's post-hoc test, where *, **, ***, and **** respectively represent $p<0.05$, $p<0.01$, $p<0.001$, and $p<0.0001$, respectively

**Supplemental Figure S3. Relative levels of 38:4-PtdInsPs to 36:x-PtdInsPs in ARPE-19 and MDA-MB-231 cells silenced for LCLAT1.** ARPE-19 cells (**A-B**) and MBA-MB-231 cells (**C-D**) were mock silenced (siCon) or LCLAT1-silenced. Cells were then grown in regular medium (control), serum-starved (ss), and stimulated with EGF for 5 min (EGF). Reactions were quenched and lipid extracted after addition of internal standards to primary cell extracts. PtdInsPs were measured by mass spectrometry (HPLC-MS). Shown is the ratio of standardized 38:4-mono-PtdIns (A, C) and 38:4-bis-PtdInsP2 (B, D) to the respective standardized sum of 36:1 and 36:2- (referred to as 36:x-PtdIns) mono-PtdInsP and bis-PtdInsP2. Lipid analysis was repeated four independent times. Shown are the mean ±STD. A two-way ANOVA and Sidak's post-hoc test was used to test data, where * is $p<0.05$. We opted to show p values in B.

**Supplemental Figure S4: MDA-MB-231 cells engineered for inducible CRISPR-Cas9 of LCLAT1.** **A.** Western blotting testing for Cas9 expression in parental MDA-MB-231 cells versus MDA-MB-231-Cas9. **B.** Western blotting testing LCLAT1 expression in MDA-MB-231-Cas9 and MDA-MB-231-Cas9 cells stably-transfected with gRNA1, gRNA2, and gRNA3 against LCLAT1. Cells were treated with 0.1 or 1 µg/mL doxycycline for 3 (shown) or 5 days. Clathrin was used as loading control **C.** Quantification of LCLAT1 expression relative to clathrin

in MDA-MB-231-Cas9 cells stably-transfected with gRNA2 after 5 days of doxycycline at indicated concentrations. **D.** Western blotting of MDA-MB-231-Cas9 cells expressing gRNA2 against LCLAT1 showing reduced LCLAT1 expression and p-Akt levels after doxycycline. **E.** Quantification of LCLAT1 expression relative to clathrin in MDA-MB-231-Cas9 cells stably-transfected with gRNA2. **F.** Quantification of p-Akt levels relative to clathrin in MDA-MB-231-Cas9 cells stably-transfected with gRNA2. All data are shown as mean±STD from three independent experiments. Data in C was tested with one-way ANOVA and Sidak's post-hoc test. Data in E and F was tested with a Mann Whitney test. * indicates $p<0.05$.

**Supplemental Video 1: Growth and cell death of MDA-MB-231 cells transiently mock silenced.** MDA-MB-231 cells were mock transfected with non-targeting siRNA and imaged in an Incucyte system in the presence of CellTox Green over 3 days at 2 frames per hour. Scale bar = 400 µm.

**Supplemental Video 2: Growth and cell death of MDA-MB-231 cells transiently silenced for LCLAT1.** MDA-MB-231 cells were silenced for LCLAT1 expression by transfected with siLCLAT1 oligonucleotides. Cells were imaged in an Incucyte system in the presence of CellTox Green over 3 days at 2 frames per hour. Scale bar = 400 µm.

**Supplemental Video 3: Growth and cell death of MDA-MB-231-Cas9 cells with no doxycycline.** MDA-MB-231-Cas9 cells in normal growth medium were imaged in an Incucyte system in the presence of CellTox Green over 3 days at 2 frames per hour. Scale bar = 400 µm.

**Supplemental Video 4: Growth and cell death of MDA-MB-231-Cas9 cells in the presence of doxycycline.** MDA-MB-231-Cas9 cells in growth medium supplemented with 1 µg/mL doxycycline were imaged in an Incucyte system in the presence of CellTox Green over 3 days at 2 frames per hour. Scale bar = 400 µm.

**Supplemental Video 5: Growth and cell death of MDA-MB-231-Cas9::gRNA2 cells without doxycycline.** MDA-MB-231-Cas9 cells stably-transfected with gRNA2 against LCLAT1 were maintained in normal growth medium and imaged in an Incucyte system in the presence of CellTox Green over 3 days at 2 frames per hour. Scale bar = 400 µm.

**Supplemental Video 6: Growth and cell death of MDA-MB-231-Cas9::gRNA2 cells in the presence of doxycycline.** MDA-MB-231-Cas9 cells stably-transfected with gRNA2 against LCLAT1 and exposed to growth medium supplemented with 1 µg/mL doxycycline were imaged in an Incucyte system in the presence of CellTox Green over 3 days at 2 frames per hour. Scale bar = 400 µm.

## References

Alessi, D. R., Deak, M., Casamayor, A., Caudwell, F. B., Morrice, N., Norman, D. G., Gaffney, P., Reese, C. B., MacDougall, C. N., Harbison, D., et al. (1997). 3-Phosphoinositide-dependent protein kinase-1 (PDK1): Structural and functional homology with the Drosophila DSTPK61 kinase. *Current Biology* 7, 776–789.

Anderson, K. E., Kielkowska, A., Durrant, T. N., Juvin, V., Clark, J., Stephens, L. R. and Hawkins, P. T. (2013). Lysophosphatidylinositol-Acyltransferase-1 (LPIAT1) Is Required to Maintain Physiological Levels of PtdIns and PtdInsP2 in the Mouse. *PLoS ONE* 8, e58425.

Anderson, K. E., Juvin, V., Clark, J., Stephens, L. R. and Hawkins, P. T. (2016). Investigating the effect of arachidonate supplementation on the phosphoinositide content of MCF10a breast epithelial cells. *Advances in biological regulation* 62, 18–24.

Balla, T. (2013). Phosphoinositides: tiny lipids with giant impact on cell regulation. *Physiological reviews* 93, 1019–137.

Barneda, D., Cosulich, S., Stephens, L. and Hawkins, P. (2019). How is the acyl chain composition of phosphoinositides created and does it matter? *Biochemical Society Transactions* 47, 1291–1305.

Bellacosa, A., Chan, T. O., Ahmed, N. N., Datta, K., Malstrom, S., Stokoe, D., McCormick, F., Feng, J. and Tsichlis, P. (1998). Akt activation by growth factors is a multiple-step process: the role of the PH domain. *Oncogene* 17, 313–325.

Bilanges, B., Posor, Y. and Vanhaesebroeck, B. (2019). PI3K isoforms in cell signalling and vesicle trafficking. *Nat Rev Mol Cell Biol* 20, 515–534.

Blunsom, N. J. and Cockcroft, S. (2020). Phosphatidylinositol synthesis at the endoplasmic reticulum. *Biochimica et Biophysica Acta - Molecular and Cell Biology of Lipids* 1865,.

Bolland, S., Pearse, R. N., Kurosaki, T. and Ravetch, J. V. (1998). SHIP modulates immune receptor responses by regulating membrane association of Btk. *Immunity* 8, 509–516.

Bone, L. N., Dayam, R. M., Lee, M., Kono, N., Fairn, G. D., Arai, H., Botelho, R. J. and Antonescu, C. N. (2017). The acyltransferase LYCAT controls specific phosphoinositides and related membrane traffic. *Molecular Biology of the Cell* 28, 161–172.

Böni-Schnetzler, M. and Pilch, P. F. (1987). Mechanism of epidermal growth factor receptor autophosphorylation and high-affinity binding. *Proc Natl Acad Sci U S A* 84, 7832–7836.

Bozelli, J. C. and Epand, R. M. (2019). Specificity of Acyl Chain Composition of Phosphatidylinositols. *Proteomics* 19,.

Bresnick, A. R. and Backer, J. M. (2019). PI3Kβ-A Versatile Transducer for GPCR, RTK, and Small GTPase Signaling. *Endocrinology* 160, 536–555.

Cabral-Dias, R., Awadeh, Y., Botelho, R. J. and Antonescu, C. N. (2021). Detection of Plasma Membrane Phosphoinositide Dynamics Using Genetically Encoded Fluorescent Protein Probes. In *Methods in Molecular Biology*, pp. 73–89. Humana Press Inc.

Cabral-Dias, R., Lucarelli, S., Zak, K., Rahmani, S., Judge, G., Abousawan, J., DiGiovanni, L. F., Vural, D., Anderson, K. E., Sugiyama, M. G., et al. (2022). Fyn and TOM1L1 are recruited to clathrin-coated pits and regulate Akt signaling. *Journal of Cell Biology* 221,.

Cao, J., Liu, Y., Lockwood, J., Burn, P. and Shi, Y. (2004). A novel cardiolipin-remodeling pathway revealed by a gene encoding an endoplasmic reticulum-associated acyl-CoA:lysocardiolipin acyltransferase (ALCAT1) in mouse. *Journal of Biological Chemistry* 279, 31727–31734.

Cao, J., Shen, W., Chang, Z. and Shi, Y. (2009). ALCAT1 is a polyglycerophospholipid acyltransferase potently regulated by adenine nucleotide and thyroid status. *American Journal of Physiology-Endocrinology and Metabolism* 296, E647–E653.

Chang, C. L. and Liou, J. (2015). Phosphatidylinositol 4, 5-bisphosphate homeostasis regulated by Nir2 and Nir3 proteins at endoplasmic reticulum-plasma membrane junctions. *Journal of Biological Chemistry* 290, 14289–14301.

Choi, S., Hedman, A. C., Sayedyahossein, S., Thapa, N., Sacks, D. B. and Anderson, R. A. (2016). Agonist-stimulated phosphatidylinositol-3,4,5-trisphosphate generation by scaffolded phosphoinositide kinases. *Nat Cell Biol* 18, 1324–1335.

Choy, C. H., Han, B. K. and Botelho, R. J. (2017). Phosphoinositide Diversity, Distribution, and Effector Function: Stepping Out of the Box. *BioEssays* 39, 1700121.

Clark, J., Anderson, K. E., Juvin, V., Smith, T. S., Karpe, F., Wakelam, M. J. O., Stephens, L. R. and Hawkins, P. T. (2011). Quantification of PtdInsP3 molecular species in cells and tissues by mass spectrometry. *Nature Methods* 8, 267–272.

Cockcroft, S., Garner, K., Yadav, S., Gomez-Espinoza, E. and Raghu, P. (2016). RdgB reciprocally transfers PA and PI at ER-PM contact sites to maintain PI(4,5)P2 homoeostasis during phospholipase C signalling in Drosophila photoreceptors. *Biochemical Society Transactions* 44, 286–292.

Cross, D. A. E., Alessi, D. R., Cohen, P., Andjelkovich, M. and Hemmings, B. A. (1995). Inhibition of glycogen synthase kinase-3 by insulin mediated by protein kinase B. *Nature* 378, 785–789.

Delos Santos, R. C., Bautista, S., Lucarelli, S., Bone, L. N., Dayam, R. M., Abousawan, J., Botelho, R. J. and Antonescu, C. N. (2017). Selective regulation of clathrin-mediated epidermal growth factor receptor signaling and endocytosis by phospholipase C and calcium. *Mol Biol Cell* 28, 2802–2818.

Dey, N., De, P. and Leyland-Jones, B. (2017). PI3K-AKT-mTOR inhibitors in breast cancers: From tumor cell signaling to clinical trials. *Pharmacology and Therapeutics* 175, 91–106.

Dibble, C. C. and Manning, B. D. (2013). Signal integration by mTORC1 coordinates nutrient input with biosynthetic output. *Nature cell biology* 15, 555–64.

Dickson, E. J. and Hille, B. (2019). Understanding phosphoinositides: rare, dynamic, and essential membrane phospholipids. *Biochem J* 476, 1–23.

Doench, J. G., Hartenian, E., Graham, D. B., Tothova, Z., Hegde, M., Smith, I., Sullender, M., Ebert, B. L., Xavier, R. J. and Root, D. E. (2014). Rational design of highly active sgRNAs for CRISPR-Cas9-mediated gene inactivation. *Nat Biotechnol* 32, 1262–1267.

Doumane, M., Caillaud, M. C. and Jaillais, Y. (2022). Experimental manipulation of phosphoinositide lipids: from cells to organisms. *Trends in Cell Biology* 32, 445–461.

Dowling, J. K. and Mansell, A. (2016). Toll-like receptors: the swiss army knife of immunity and vaccine development. *Clinical & Translational Immunology* 5, e85.

D'Souza, K. and Epand, R. M. (2014). Enrichment of phosphatidylinositols with specific acyl chains. *Biochim. Biophys. Acta - Biomembr.* 1838, 1501–1508.

Duncan, L., Shay, C. and Teng, Y. (2020). PI3K Isoform-Selective Inhibitors in Cancer. *Adv Exp Med Biol* 1255, 165–173.

Frank, S. B., Schulz, V. V. and Miranti, C. K. (2017). A streamlined method for the design and cloning of shRNAs into an optimized Dox-inducible lentiviral vector. *BMC Biotechnol* 17, 24.

Freyr Eiriksson, F., Kampp Nøhr, M., Costa, M., Klara Bö dvarsdottir, S., Margret, H. O. and Thorsteinsdottir, M. (2020). Lipidomic study of cell lines reveals differences between breast cancer subtypes.

Getahun, A. and Cambier, J. C. (2015). Of ITIMs, ITAMs, and ITAMis: Revisiting immunoglobulin Fc receptor signaling. *Immunological Reviews* 268, 66–73.

Gullick, W. J., Downward, J. and Waterfield, M. D. (1985). Antibodies to the autophosphorylation sites of the epidermal growth factor receptor protein-tyrosine kinase as probes of structure and function. *EMBO J* 4, 2869–2877.

Haag, M., Schmidt, A., Sachsenheimer, T. and Brügger, B. (2012). Quantification of Signaling Lipids by Nano-Electrospray Ionization Tandem Mass Spectrometry (Nano-ESI MS/MS). *Metabolites* 2, 57–76.

Hammond, G. R. V., Fischer, M. J., Anderson, K. E., Holdich, J., Koteci, A., Balla, T. and Irvine, R. F. (2012). PI4P and PI(4,5)P2 are essential but independent lipid determinants of membrane identity. *Science (New York, N.Y.)* 337, 727–30.

Haugh, J. M., Codazzi, F., Teruel, M. and Meyer, T. (2000). Spatial Sensing in Fibroblasts Mediated by 3′ Phosphoinositides. *Journal of Cell Biology* 151, 1269–1280.

Hicks, A. M., DeLong, C. J., Thomas, M. J., Samuel, M. and Cui, Z. (2006). Unique molecular signatures of glycerophospholipid species in different rat tissues analyzed by tandem mass spectrometry. *Biochimica et Biophysica Acta (BBA) - Molecular and Cell Biology of Lipids* 1761, 1022–1029.

Holgado-Madruga, M., Emlet, D. R., Moscatello, D. K., Godwin, A. K. and Wong, A. J. (1996). A Grb2-associated docking protein in EGF- and insulin-receptor signalling. *Nature* 379, 560–564.

Honegger, A. M., Szapary, D., Schmidt, A., Lyall, R., Van Obberghen, E., Dull, T. J., Ullrich, A. and Schlessinger, J. (1987). A mutant epidermal growth factor receptor with defective protein tyrosine kinase is unable to stimulate proto-oncogene expression and DNA synthesis. *Mol Cell Biol* 7, 4568–4571.

Hu, P., Margolis, B., Skolnik, E. Y., Lammers, R., Ullrich, A. and Schlessinger, J. (1992). Interaction of phosphatidylinositol 3-kinase-associated p85 with epidermal growth factor and platelet-derived growth factor receptors. *Mol Cell Biol* 12, 981–990.

Huang, L. S., Mathew, B., Li, H., Zhao, Y., Ma, S. F., Noth, I., Reddy, S. P., Harijith, A., Usatyuk, P. V., Berdyshev, E. V., et al. (2014). The mitochondrial cardiolipin remodeling enzyme lysocardiolipin acyltransferase is a novel target in pulmonary fibrosis. *American Journal of Respiratory and Critical Care Medicine* 189, 1402–1415.

Huang, L. S., Jiang, P., Feghali-Bostwick, C., Reddy, S. P., Garcia, J. G. N. and Natarajan, V. (2017). Lysocardiolipin acyltransferase regulates TGF-β mediated lung fibroblast differentiation. *Free Radical Biology and Medicine* 112, 162–173.

Huang, L. S., Kotha, S. R., Avasarala, S., VanScoyk, M., Winn, R. A., Pennathur, A., Yashaswini, P. S., Bandela, M., Salgia, R., Tyurina, Y. Y., et al. (2020). Lysocardiolipin acyltransferase regulates NSCLC cell proliferation and migration by modulating mitochondrial dynamics. *Journal of Biological Chemistry* 295, 13393–13406.

Idevall-Hagren, O. and De Camilli, P. (2015). Detection and manipulation of phosphoinositides. *Biochimica et Biophysica Acta - Molecular and Cell Biology of Lipids* 1851, 736–745.

Imae, R., Inoue, T., Nakasaki, Y., Uchida, Y., Ohba, Y., Kono, N., Nakanishi, H., Sasaki, T., Mitani, S. and Arai, H. (2012). LYCAT, a homologue of *C. elegans acl-8* , *acl-9* , and *acl-10* , determines the fatty acid composition of phosphatidylinositol in mice. *Journal of Lipid Research* 53, 335–347.

Inoki, K., Li, Y., Zhu, T., Wu, J. and Guan, K.-L. (2002). TSC2 is phosphorylated and inhibited by Akt and suppresses mTOR signalling. *Nature Cell Biology* 4, 648–657.

Inoki, K., Li, Y., Xu, T. and Guan, K. L. (2003). Rheb GTpase is a direct target of TSC2 GAP activity and regulates mTOR signaling. *Genes and Development* 17, 1829–1834.

Katan, M. and Cockcroft, S. (2020). Phosphatidylinositol(4,5)bisphosphate: diverse functions at the plasma membrane. *Essays in Biochemistry* 20200041.

Kim, Y. J., Guzman-Hernandez, M.-L., Wisniewski, E. and Balla, T. (2015). Phosphatidylinositol-Phosphatidic Acid Exchange by Nir2 at ER-PM Contact Sites Maintains Phosphoinositide Signaling Competence. *Developmental Cell* 33, 549–561.

Kiyatkin, A., Aksamitiene, E., Markevich, N. I., Borisov, N. M., Hoek, J. B. and Kholodenko, B. N. (2006). Scaffolding protein Grb2-associated binder 1 sustains epidermal growth factor-induced mitogenic and survival signaling by multiple positive feedback loops. *Journal of Biological Chemistry* 281, 19925–19938.

Koizumi, A., Narita, S., Nakanishi, H., Ishikawa, M., Eguchi, S., Kimura, H., Takasuga, S., Huang, M., Inoue, T., Sasaki, J., et al. (2019). Increased fatty acyl saturation of phosphatidylinositol phosphates in prostate cancer progression. *Scientific Reports* 9, 1–8.

Koland, J. G. and Cerione, R. A. (1988). Growth factor control of epidermal growth factor receptor kinase activity via an intramolecular mechanism. *J Biol Chem* 263, 2230–2237.

Lee, H.-C., Inoue, T., Sasaki, J., Kubo, T., Matsuda, S., Nakasaki, Y., Hattori, M., Tanaka, F., Udagawa, O., Kono, N., et al. (2012). LPIAT1 regulates arachidonic acid content in phosphatidylinositol and is required for cortical lamination in mice. *Molecular biology of the cell* 23, 4689–700.

Lees, J. A., Messa, M., Sun, E. W., Wheeler, H., Torta, F., Wenk, M. R., De Camilli, P. and Reinisch, K. M. (2017). Lipid transport by TMEM24 at ER-plasma membrane contacts regulates pulsatile insulin secretion. *Science* 355, eaah6171.

Li, J., Romestaing, C., Han, X., Li, Y., Hao, X., Wu, Y., Sun, C., Liu, X., Jefferson, L. S., Xiong, J., et al. (2010). Cardiolipin remodeling by ALCAT1 links oxidative stress and mitochondrial dysfunction to obesity. *Cell Metabolism* 12, 154–165.

Li, J., Liu, X., Wang, H., Zhang, W., Chan, D. C. and Shi, Y. (2012). Lysocardiolipin acyltransferase 1 (ALCAT1) controls mitochondrial DNA fidelity and biogenesis through modulation of MFN2 expression. *Proceedings of the National Academy of Sciences of the United States of America* 109, 6975–6980.

Li, S., Shen, Y., Wang, M., Yang, J., Lv, M., Li, P., Chen, Z. and Yang, J. (2017). Loss of PTEN expression in breast cancer: association with clinicopathological characteristics and prognosis. *Oncotarget* 8, 32043–32054.

Lien, E. C., Dibble, C. C. and Toker, A. (2017). PI3K signaling in cancer: beyond AKT. *Current Opinion in Cell Biology* 45, 62–71.

Linggi, B. and Carpenter, G. (2006). ErbB receptors: new insights on mechanisms and biology. *Trends in Cell Biology* 16, 649–656.

Liu, X., Ye, B., Miller, S., Yuan, H., Zhang, H., Tian, L., Nie, J., Imae, R., Arai, H., Li, Y., et al. (2012). Ablation of ALCAT1 Mitigates Hypertrophic Cardiomyopathy through Effects on Oxidative Stress and Mitophagy. *Molecular and Cellular Biology* 32, 4493–4504.

Manning, B. D. and Toker, A. (2017). AKT/PKB Signaling: Navigating the Network. *Cell* 169, 381–405.

Margolis, B., Bellot, F., Honegger, A. M., Ullrich, A., Schlessinger, J. and Zilberstein, A. (1990a). Tyrosine kinase activity is essential for the association of phospholipase C-gamma with the epidermal growth factor receptor. *Mol Cell Biol* 10, 435–441.

Margolis, B., Li, N., Koch, A., Mohammadi, M., Hurwitz, D. R., Zilberstein, A., Ullrich, A., Pawson, T. and Schlessinger, J. (1990b). The tyrosine phosphorylated carboxyterminus of the EGF receptor is a binding site for GAP and PLC-gamma. *EMBO J* 9, 4375–4380.

Marshall, J. G., Booth, J. W., Stambolic, V., Mak, T., Balla, T., Schreiber, A. D., Meyer, T. and Grinstein, S. (2001). Restricted accumulation of phosphatidylinositol 3-kinase products in a plasmalemmal subdomain during Fc?? receptor-mediated phagocytosis. *Journal of Cell Biology* 153, 1369–1380.

Milne, S. B., Ivanova, P. T., DeCamp, D., Hsueh, R. C. and Brown, H. A. (2005). A targeted mass spectrometric analysis of phosphatidylinositol phosphate species. *J Lipid Res* 46, 1796–1802.

Morioka, S., Nakanishi, H., Yamamoto, T., Hasegawa, J., Tokuda, E., Hikita, T., Sakihara, T., Kugii, Y., Oneyama, C., Yamazaki, M., et al. (2022). A mass spectrometric method for in-depth profiling of phosphoinositide regioisomers and their disease-associated regulation. *Nat Commun* 13, 83.

Mujalli, A., Chicanne, G., Bertrand-Michel, J., Viars, F., Stephens, L., Hawkins, P., Viaud, J., Gaits-Iacovoni, F., Severin, S., Gratacap, M. P., et al. (2018). Profiling of phosphoinositide molecular species in human and mouse platelets identifies new species increasing following stimulation. *Biochimica et Biophysica Acta - Molecular and Cell Biology of Lipids* 1863, 1121–1131.

Naguib, A., Bencze, G., Engle, D. D., Chio, I. I. C., Herzka, T., Watrud, K., Bencze, S., Tuveson, D. A., Pappin, D. J. and Trotman, L. C. (2015). P53 mutations change phosphatidylinositol acyl chain composition. *Cell Reports* 10, 8–19.

Ohashi, Y., Tremel, S., Masson, G. R., McGinney, L., Boulanger, J., Rostislavleva, K., Johnson, C. M., Niewczas, I., Clark, J. and Williams, R. L. (2020). Membrane characteristics tune activities of endosomal and autophagic human VPS34 complexes. *eLife* 9, e58281.

Orofiamma, L. A., Vural, D. and Antonescu, C. N. (2022). Control of cell metabolism by the epidermal growth factor receptor. *Biochim Biophys Acta Mol Cell Res* 119359.

Pemberton, J. G., Kim, Y. J., Humpolickova, J., Eisenreichova, A., Sengupta, N., Toth, D. J., Boura, E. and Balla, T. (2020). Defining the subcellular distribution and metabolic channeling of phosphatidylinositol. *Journal of Cell Biology* 219,.

Posor, Y., Jang, W. and Haucke, V. (2022). Phosphoinositides as membrane organizers. *Nat Rev Mol Cell Biol*.

Rodgers, S. J., Ferguson, D. T., Mitchell, C. A. and Ooms, L. M. (2017). Regulation of PI3K effector signalling in cancer by the phosphoinositide phosphatases. *Bioscience Reports* 37, BSR20160432.

Rodrigues, G. A., Falasca, M., Zhang, Z., Ong, S. H. and Schlessinger, J. (2000). A novel positive feedback loop mediated by the docking protein Gab1 and phosphatidylinositol 3-kinase in epidermal growth factor receptor signaling. *Mol Cell Biol* 20, 1448–1459.

Rueda-Rincon, N., Bloch, K., Derua, R., Vyas, R., Harms, A., Hankemeier, T., Ali Khan, N., Dehairs, J., Bagadi, M., Mercedes Binda, M., et al. (2015). p53 attenuates AKT signaling by modulating membrane phospholipid composition. *Oncotarget* 6, 21240–21254.

Saheki, Y., Bian, X., Schauder, C. M., Sawaki, Y., Surma, M. A., Klose, C., Pincet, F., Reinisch, K. M. and De Camilli, P. (2016). Control of plasma membrane lipid homeostasis by the extended synaptotagmins. *Nature Cell Biology* 18, 504–515.

Salamon, R. S. and Backer, J. M. (2013). Phosphatidylinositol-3,4,5-trisphosphate: Tool of choice for class I PI 3-kinases. *BioEssays: news and reviews in molecular, cellular and developmental biology* 35, 602–11.

Sanjana, N. E., Shalem, O. and Zhang, F. (2014). Improved vectors and genome-wide libraries for CRISPR screening. *Nat Methods* 11, 783–784.

Schindelin, J., Arganda-Carreras, I., Frise, E., Kaynig, V., Longair, M., Pietzsch, T., Preibisch, S., Rueden, C., Saalfeld, S., Schmid, B., et al. (2012). Fiji: An open-source platform for biological-image analysis. *Nature Methods* 9, 676–682.

Schmid, A. C., Wise, H. M., Mitchell, C. A., Nussbaum, R. and Woscholski, R. (2004). Type II phosphoinositide 5-phosphatases have unique sensitivities towards fatty acid composition and head group phosphorylation. *FEBS Letters* 576, 9–13.

Shulga, Y. V., Anderson, R. A., Topham, M. K. and Epand, R. M. (2012). Phosphatidylinositol-4-phosphate 5-kinase isoforms exhibit acyl chain selectivity for both substrate and lipid activator. *J. Biol. Chem.* 287, 35953–35963.

Stokoe, D., Stephens, L. R., Copeland, T., Gaffney, P. R. J., Reese, C. B., Painter, G. F., Holmes, A. B., McCormick, F. and Hawkins, P. T. (1997). Dual role of phosphatidylinositol-3,4,5-trisphosphate in the activation of protein kinase B. *Science* 277, 567–570.

Sugiyama, M. G., Fairn, G. D. and Antonescu, C. N. (2019). Akt-ing Up Just About Everywhere: Compartment-Specific Akt Activation and Function in Receptor Tyrosine Kinase Signaling. *Front Cell Dev Biol* 7, 70.

Sun, Y., Thapa, N., Hedman, A. C. and Anderson, R. a (2013). Phosphatidylinositol 4,5-bisphosphate: targeted production and signaling. *BioEssays : news and reviews in molecular, cellular and developmental biology* 35, 513–22.

Takeuchi, K. and Ito, F. (2011). Receptor tyrosine kinases and targeted cancer therapeutics. *Biol Pharm Bull* 34, 1774–1780.

Traynor-Kaplan, A., Kruse, M., Dickson, E. J., Dai, G., Vivas, O., Yu, H., Whittington, D. and Hille, B. (2017). Fatty-acyl chain profiles of cellular phosphoinositides. *Biochimica et Biophysica Acta - Molecular and Cell Biology of Lipids* 1862, 513–522.

Várnai, P. and Balla, T. (1998). Visualization of phosphoinositides that bind pleckstrin homology domains: Calcium- and agonist-induced dynamic changes and relationship to myo-[3H]inositol-labeled phosphoinositide pools. *Journal of Cell Biology* 143, 501–510.

Wang, S. E., Shin, I., Wu, F. Y., Friedman, D. B. and Arteaga, C. L. (2006). HER2/Neu (ErbB2) signaling to Rac1-Pak1 is temporally and spatially modulated by transforming growth factor beta. *Cancer Res* 66, 9591–9600.

Wang, C., Faloon, P. W., Tan, Z., Lv, Y., Zhang, P., Ge, Y., Deng, H. and Xiong, J. W. (2007). Mouse lysocardiolipin acyltransferase controls the development of hematopoietic and endothelial lineages during in vitro embryonic stem-cell differentiation. *Blood* 110, 3601–3609.

Xiong, J. W., Yu, Q., Zhang, J. and Mably, J. D. (2008). An acyltransferase controls the generation of hematopoietic and endothelial lineages in zebrafish. *Circulation Research* 102, 1057–1064.

Yarden, Y. and Schlessinger, J. (1987). Epidermal growth factor induces rapid, reversible aggregation of the purified epidermal growth factor receptor. *Biochemistry* 26, 1443–1451.

Zaman, M. F., Nenadic, A., Radojičić, A., Rosado, A. and Beh, C. T. (2020). Sticking With It: ER-PM Membrane Contact Sites as a Coordinating Nexus for Regulating Lipids and Proteins at the Cell Cortex. *Frontiers in Cell and Developmental Biology* 8,.

Zewe, J. P., Miller, A. M., Sangappa, S., Wills, R. C., Goulden, B. D. and Hammond, G. R. V. (2020). Probing the subcellular distribution of phosphatidylinositol reveals a surprising lack at the plasma membrane. *Journal of Cell Biology* 219,.

Zhu, G., Fan, Z., Ding, M., Zhang, H., Mu, L., Ding, Y., Zhang, Y., Jia, B., Chen, L., Chang, Z., et al. (2015). An EGFR/PI3K/AKT axis promotes accumulation of the Rac1-GEF Tiam1 that is critical in EGFR-driven tumorigenesis. *Oncogene* 34, 5971–5982.

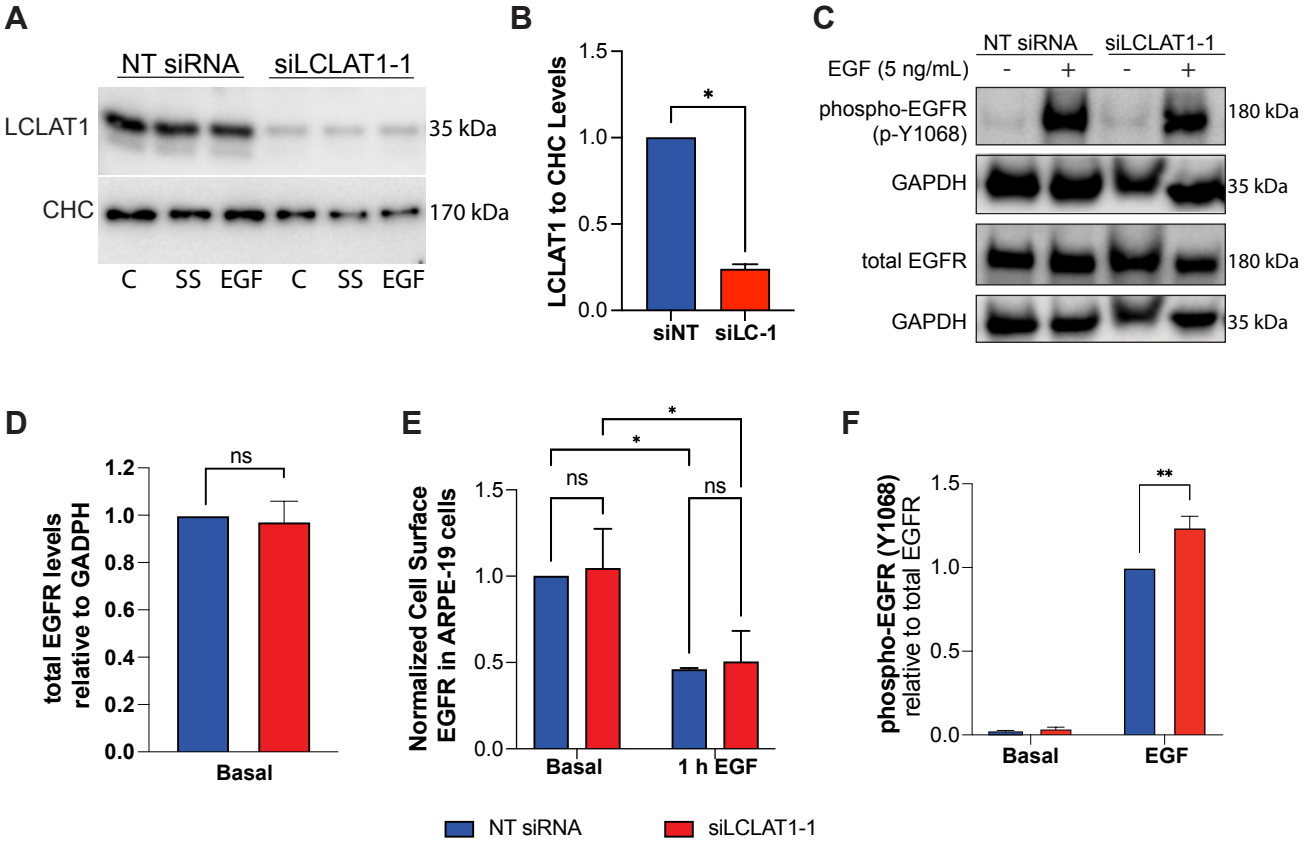
A
NT siRNA
siLCLAT1-1
LCLAT1
35 kDa
CHC
170 kDa
C
SS
EGF
C
SS
EGF
B
LCLAT1 to CHC Levels
1.5
1.0
0.5
0.0
*
siNT
siLC-1
C
NT siRNA
siLCLAT1-1
EGF (5 ng/mL)
-
+
-
+
phospho-EGFR
(p-Y1068)
180 kDa
GAPDH
35 kDa
total EGFR
180 kDa
GAPDH
35 kDa
D
total EGFR levels
relative to GADPH
1.2
1.0
0.8
0.6
0.4
0.2
0.0
ns
Basal
E
Normalized Cell Surface
EGFR in ARPE-19 cells
1.5
1.0
0.5
0.0
*
*
ns
ns
Basal
1 h EGF
F
phospho-EGFR (Y1068)
relative to total EGFR
1.5
1.0
0.5
0.0
**
Basal
EGF
NT siRNA
siLCLAT1-1

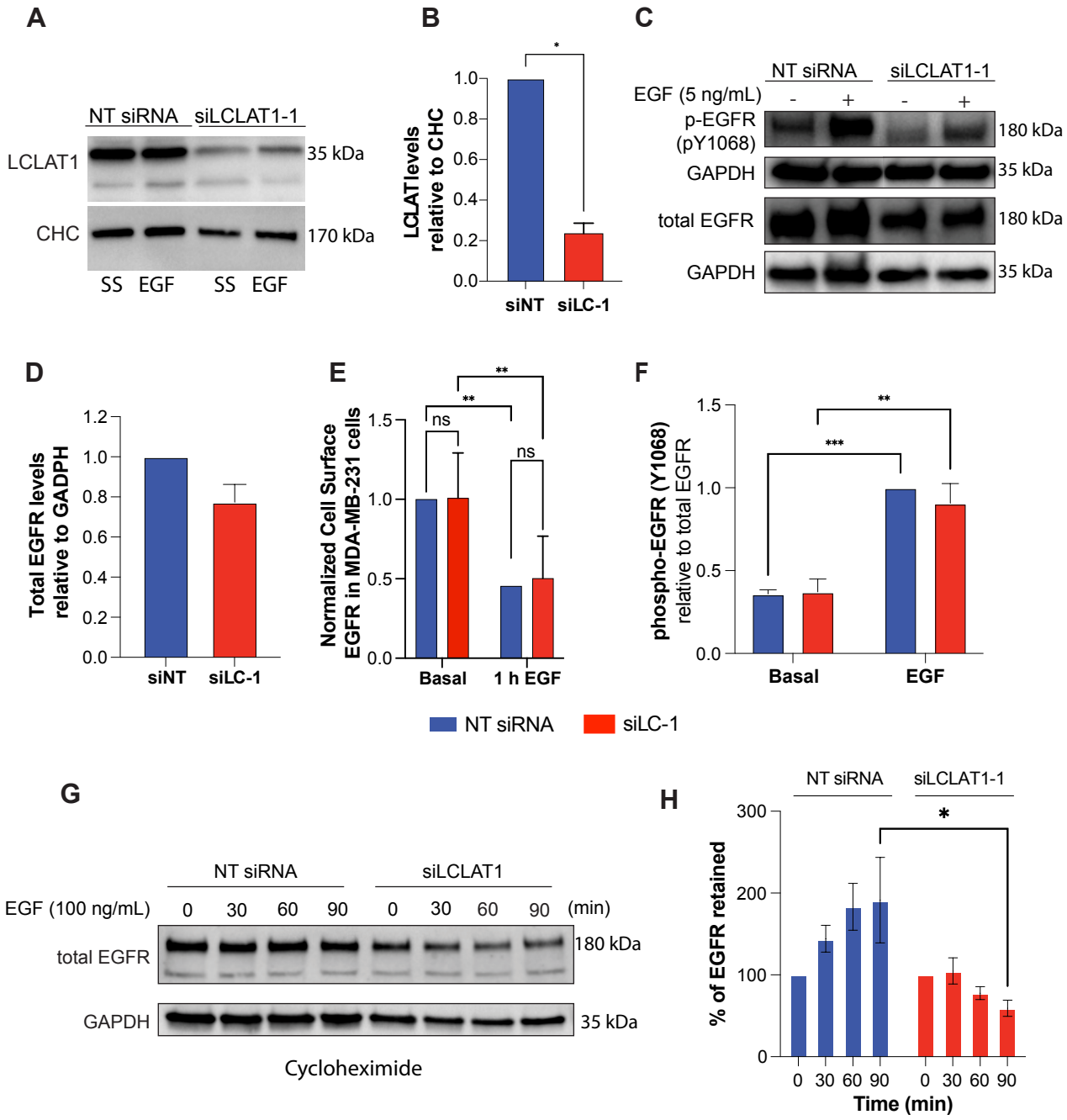
A
NT siRNA
siLCLAT1-1
LCLAT1
35 kDa
CHC
170 kDa
SS
EGF
SS
EGF
B
LCLAT levels relative to CHC
1.0
0.8
0.6
0.4
0.2
0.0
*
siNT
siLC-1
C
NT siRNA
siLCLAT1-1
EGF (5 ng/mL)
-
+
-
+
p-EGFR (pY1068)
180 kDa
GAPDH
35 kDa
total EGFR
180 kDa
GAPDH
35 kDa
D
Total EGFR levels relative to GADPH
1.2
1.0
0.8
0.6
0.4
0.2
0.0
siNT
siLC-1
E
Normalized Cell Surface EGFR in MDA-MB-231 cells
1.5
1.0
0.5
0.0
ns
**
**
ns
Basal
1 h EGF
F
phospho-EGFR (Y1068) relative to total EGFR
1.5
1.0
0.5
0.0
**
***
Basal
EGF
NT siRNA
siLC-1
G
NT siRNA
siLCLAT1
EGF (100 ng/mL)
0
30
60
90
0
30
60
90
(min)
total EGFR
180 kDa
GAPDH
35 kDa
Cycloheximide
H
NT siRNA
siLCLAT1-1
*
% of EGFR retained
300
200
100
0
0
30
60
90
0
30
60
90
Time (min)

Figure 2

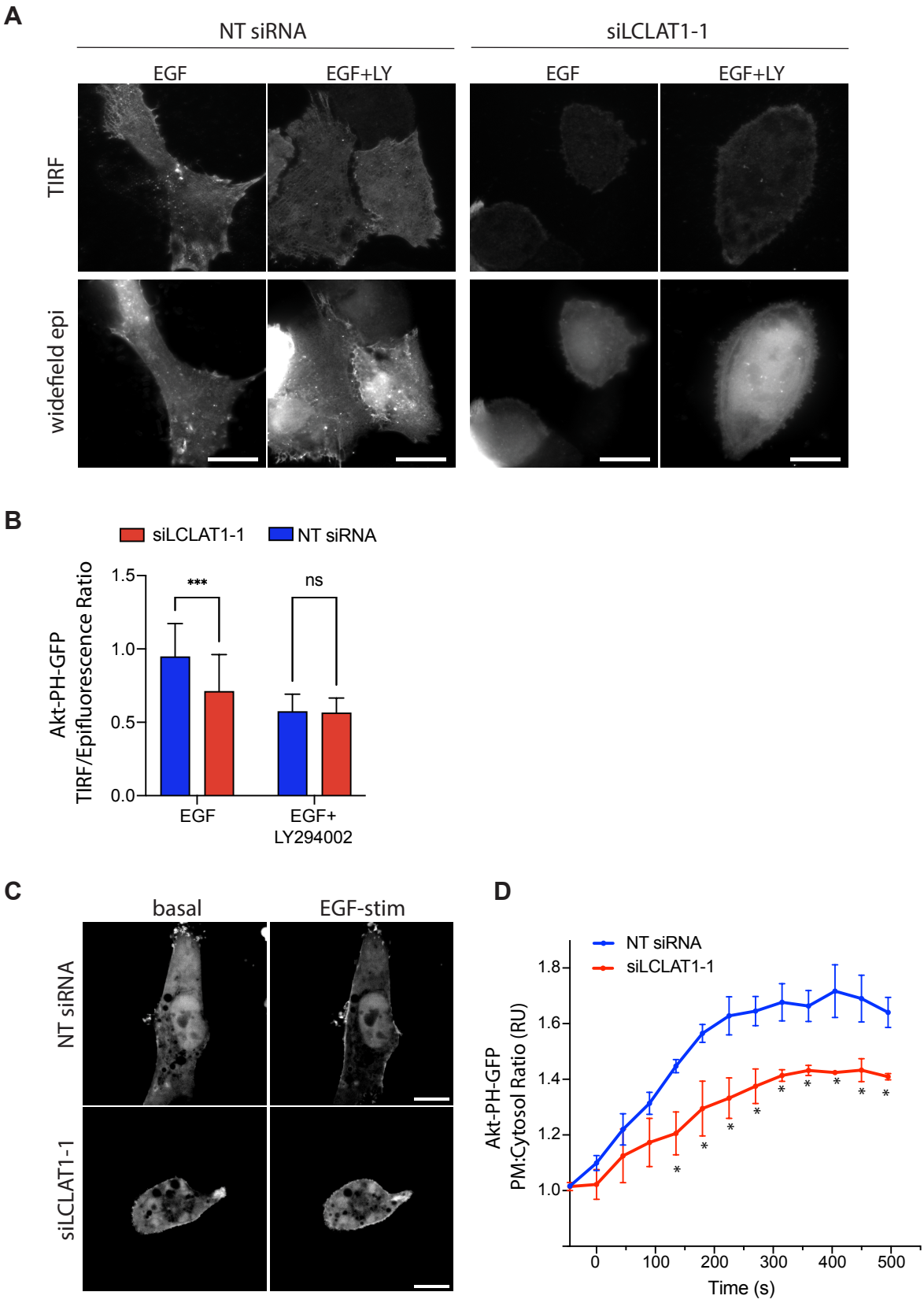
A
NT siRNA
siLCLAT1-1
EGF
EGF+LY
EGF
EGF+LY
TIRF
widefield epi
B
siLCLAT1-1
NT siRNA
Akt-PH-GFP
TIRF/Epifluorescence Ratio
1.5
1.0
0.5
0.0
***
ns
EGF
EGF+
LY294002
C
basal
EGF-stim
NT siRNA
siLCLAT1-1
D
NT siRNA
siLCLAT1-1
Akt-PH-GFP
PM:Cytosol Ratio (RU)
1.8
1.6
1.4
1.2
1.0
0
100
200
300
400
500
Time (s)

Figure 3

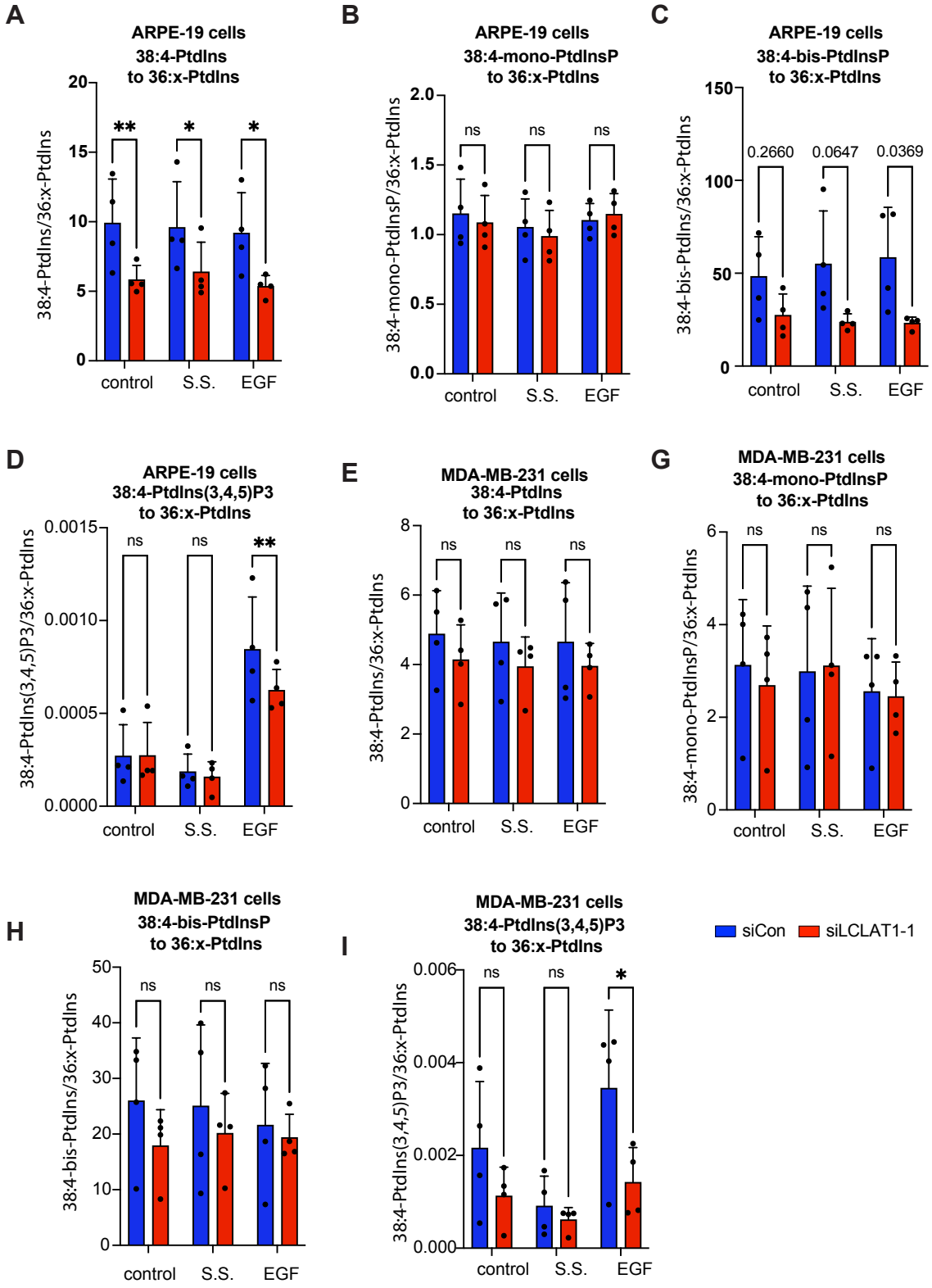
A
ARPE-19 cells
38:4-PtdIns
to 36:x-PtdIns
38:4-PtdIns/36:x-PtdIns
control
S.S.
EGF
B
ARPE-19 cells
38:4-mono-PtdInsP
to 36:x-PtdIns
38:4-mono-PtdInsP/36:x-PtdIns
C
ARPE-19 cells
38:4-bis-PtdInsP
to 36:x-PtdIns
38:4-bis-PtdIns/36:x-PtdIns
0.2660
0.0647
0.0369
D
ARPE-19 cells
38:4-PtdIns(3,4,5)P3
to 36:x-PtdIns
38:4-PtdIns(3,4,5)P3/36:x-PtdIns
E
MDA-MB-231 cells
38:4-PtdIns
to 36:x-PtdIns
G
MDA-MB-231 cells
38:4-mono-PtdInsP
to 36:x-PtdIns
H
MDA-MB-231 cells
38:4-bis-PtdInsP
to 36:x-PtdIns
I
MDA-MB-231 cells
38:4-PtdIns(3,4,5)P3
to 36:x-PtdIns
siCon
siLCLAT1-1

Figure 4

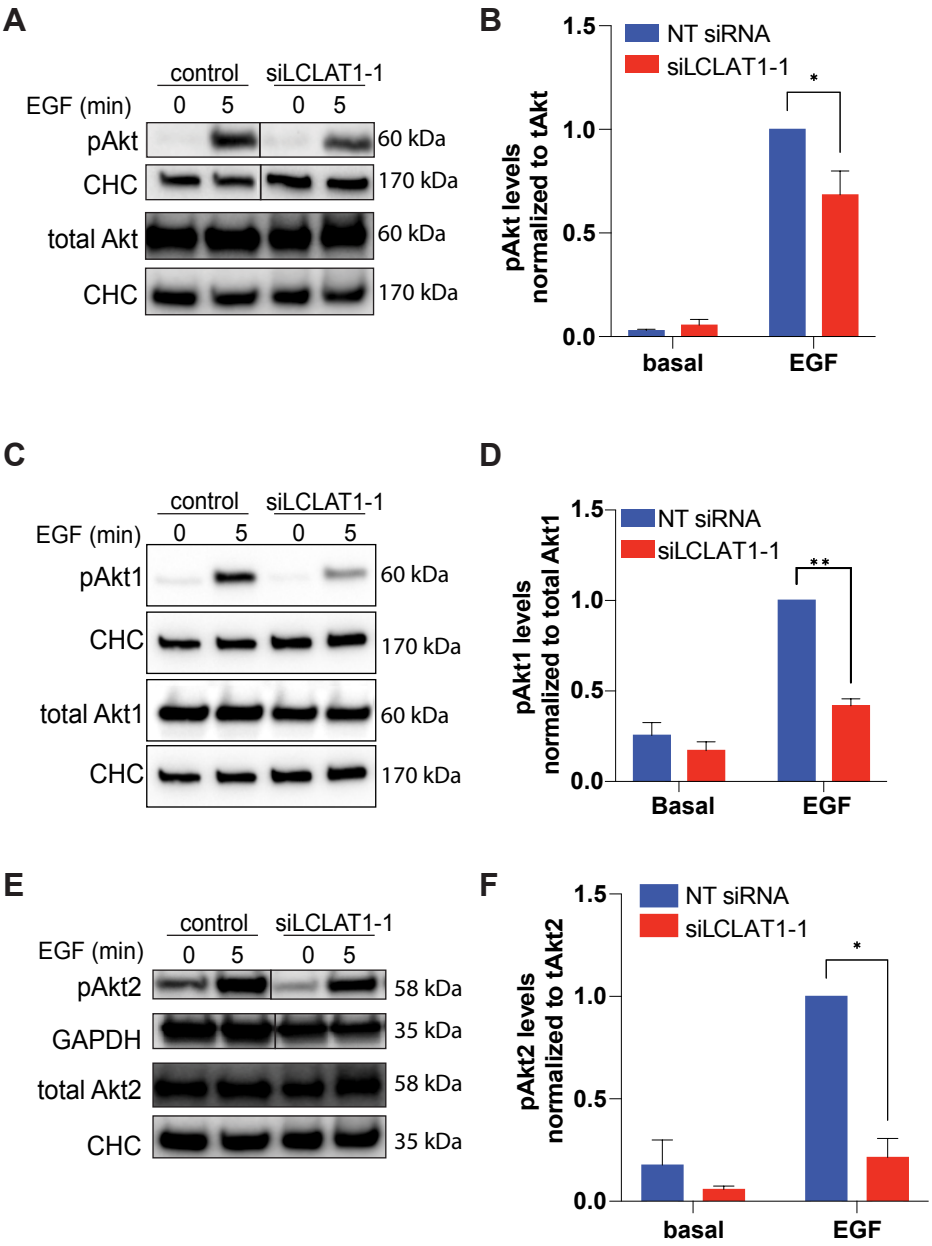
A
control
siLCLAT1-1
EGF (min)
0
5
0
5
pAkt
60 kDa
CHC
170 kDa
total Akt
60 kDa
CHC
170 kDa
B
NT siRNA
siLCLAT1-1
pAkt levels normalized to tAkt
1.5
1.0
0.5
0.0
*
basal
EGF
C
control
siLCLAT1-1
EGF (min)
0
5
0
5
pAkt1
60 kDa
CHC
170 kDa
total Akt1
60 kDa
CHC
170 kDa
D
NT siRNA
siLCLAT1-1
pAkt1 levels normalized to total Akt1
1.5
1.0
0.5
0.0
**
Basal
EGF
E
control
siLCLAT1-1
EGF (min)
0
5
0
5
pAkt2
58 kDa
GAPDH
35 kDa
total Akt2
58 kDa
CHC
35 kDa
F
NT siRNA
siLCLAT1-1
pAkt2 levels normalized to tAkt2
1.5
1.0
0.5
0.0
*
basal
EGF

**Figure 5**

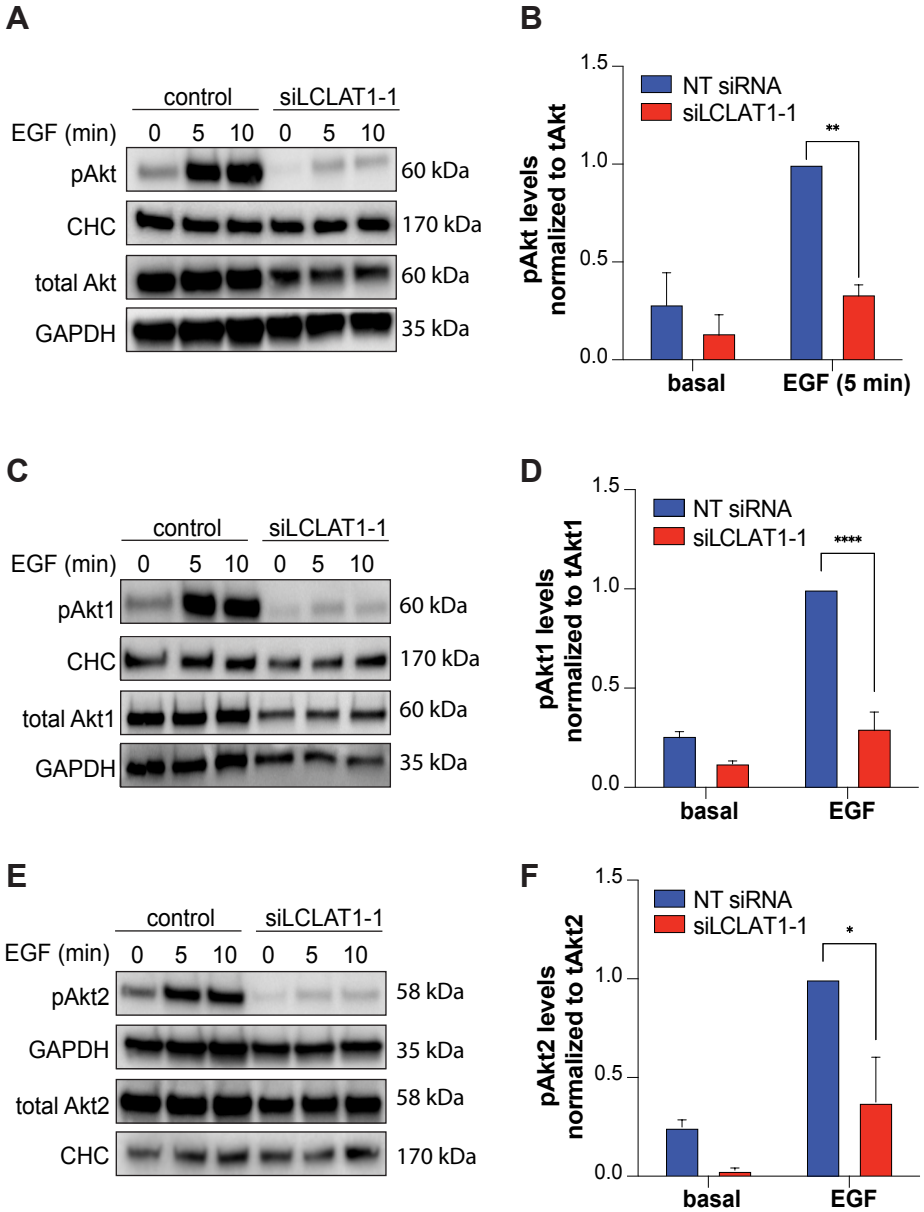
A
control
siLCLAT1-1
EGF (min)
0 5 10 0 5 10
pAkt
CHC
total Akt
GAPDH
60 kDa
170 kDa
60 kDa
35 kDa
B
NT siRNA
siLCLAT1-1
pAkt levels normalized to tAkt
1.5
1.0
0.5
0.0
**
basal
EGF (5 min)
C
control
siLCLAT1-1
EGF (min)
0 5 10 0 5 10
pAkt1
CHC
total Akt1
GAPDH
60 kDa
170 kDa
60 kDa
35 kDa
D
NT siRNA
siLCLAT1-1
pAkt1 levels normalized to tAkt1
1.5
1.0
0.5
0.0
****
basal
EGF
E
control
siLCLAT1-1
EGF (min)
0 5 10 0 5 10
pAkt2
GAPDH
total Akt2
CHC
58 kDa
35 kDa
58 kDa
170 kDa
F
NT siRNA
siLCLAT1-1
pAkt2 levels normalized to tAkt2
1.5
1.0
0.5
0.0
*
basal
EGF

Figure 6

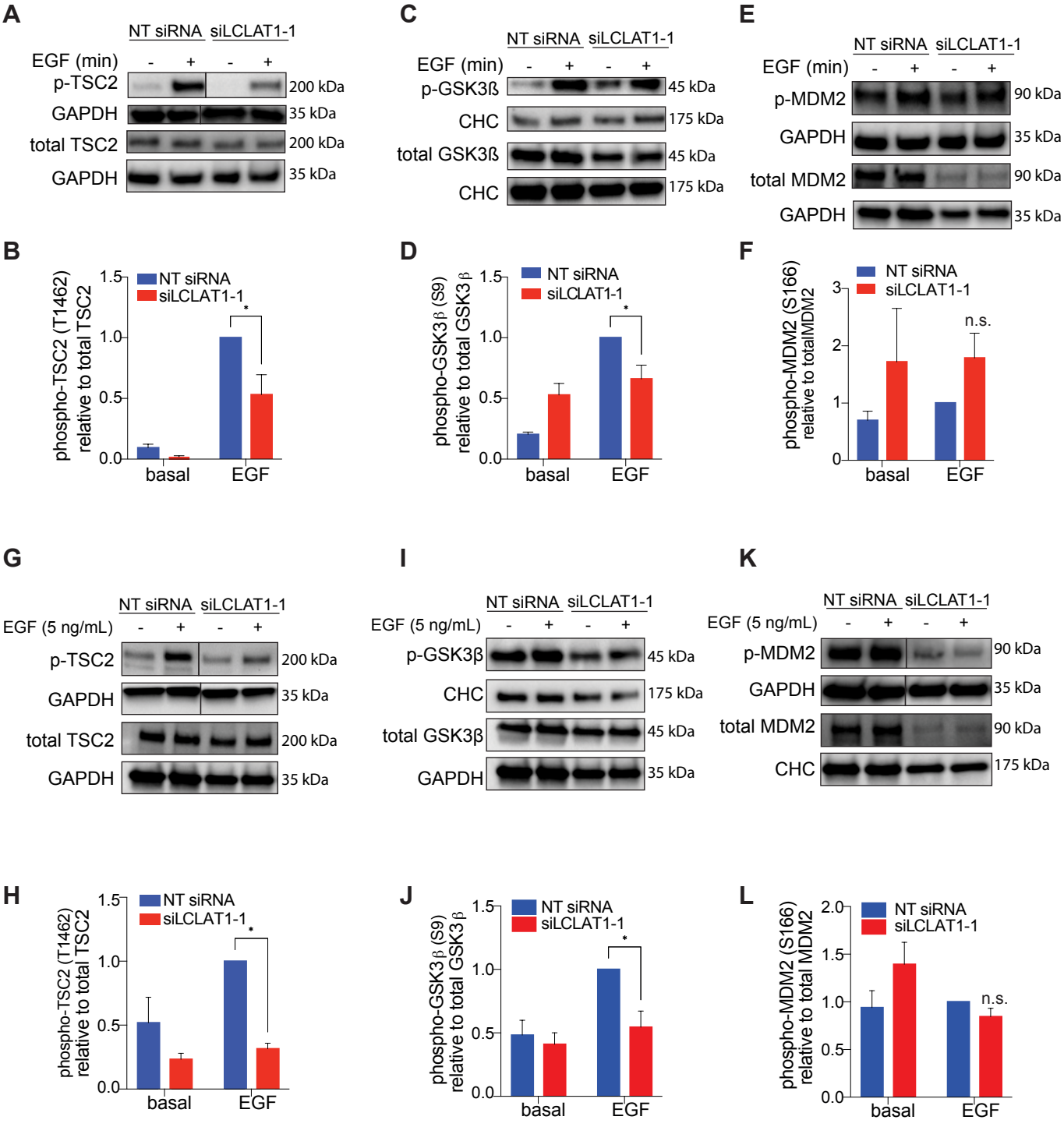
A
NT siRNA siLCLAT1-1
EGF (min) - + - +
p-TSC2 200 kDa
GAPDH 35 kDa
total TSC2 200 kDa
GAPDH 35 kDa
B
phospho-TSC2 (T1462) relative to total TSC2
NT siRNA
siLCLAT1-1
basal EGF
C
NT siRNA siLCLAT1-1
EGF (min) - + - +
p-GSK3ß 45 kDa
CHC 175 kDa
total GSK3ß 45 kDa
CHC 175 kDa
D
phospho-GSK3β (S9) relative to total GSK3β
NT siRNA
siLCLAT1-1
basal EGF
E
NT siRNA siLCLAT1-1
EGF (min) - + - +
p-MDM2 90 kDa
GAPDH 35 kDa
total MDM2 90 kDa
GAPDH 35 kDa
F
phospho-MDM2 (S166) relative to totalMDM2
NT siRNA
siLCLAT1-1
n.s.
basal EGF
G
NT siRNA siLCLAT1-1
EGF (5 ng/mL) - + - +
p-TSC2 200 kDa
GAPDH 35 kDa
total TSC2 200 kDa
GAPDH 35 kDa
H
phospho-TSC2 (T1462) relative to total TSC2
NT siRNA
siLCLAT1-1
basal EGF
I
NT siRNA siLCLAT1-1
EGF (5 ng/mL) - + - +
p-GSK3β 45 kDa
CHC 175 kDa
total GSK3β 45 kDa
GAPDH 35 kDa
J
phospho-GSK3β (S9) relative to total GSK3β
NT siRNA
siLCLAT1-1
basal EGF
K
NT siRNA siLCLAT1-1
EGF (5 ng/mL) - + - +
p-MDM2 90 kDa
GAPDH 35 kDa
total MDM2 90 kDa
CHC 175 kDa
L
phospho-MDM2 (S166) relative to total MDM2
NT siRNA
siLCLAT1-1
n.s.
basal EGF

Figure 7

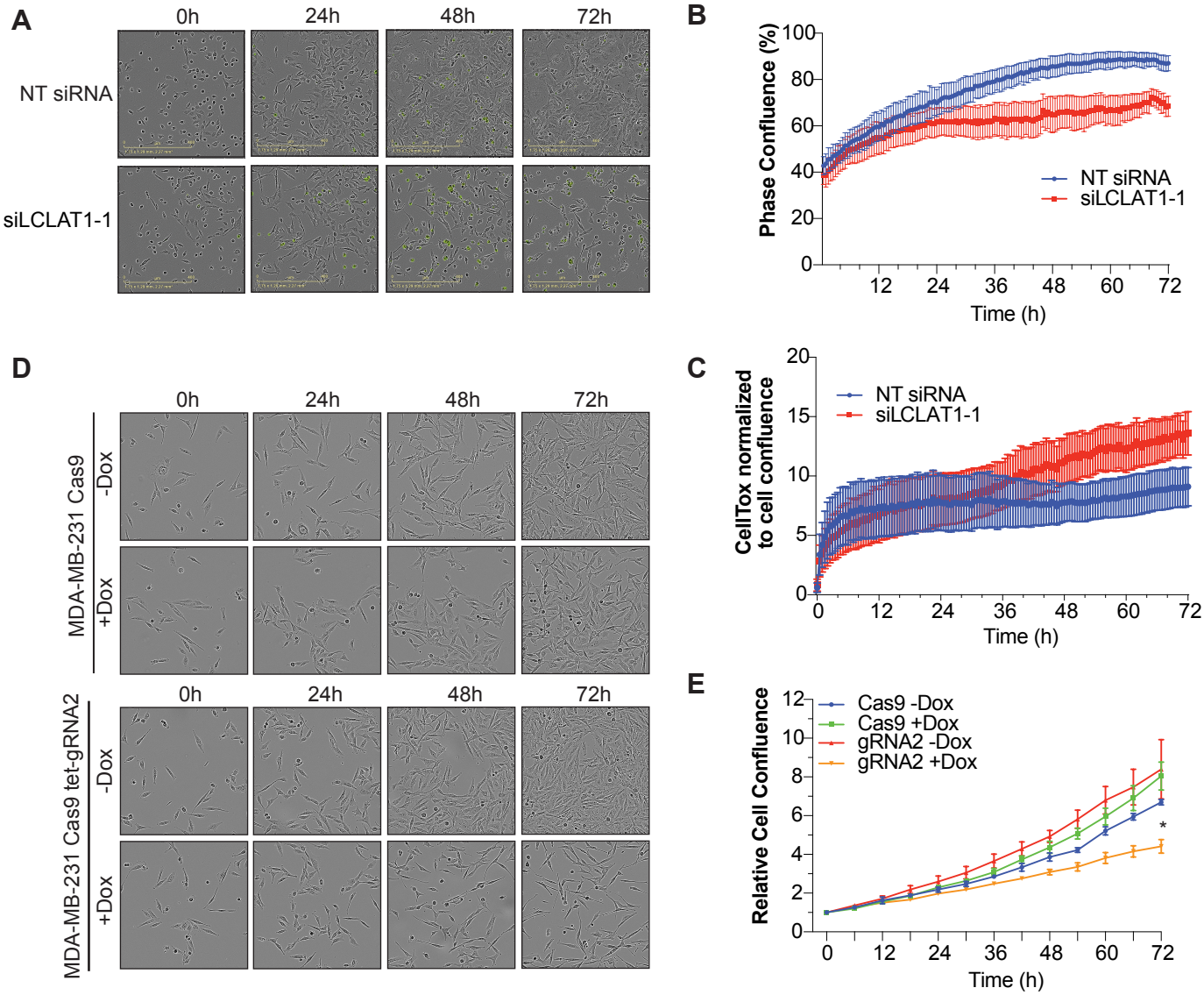
A
0h
24h
48h
72h
NT siRNA
siLCLAT1-1
B
Phase Confluence (%)
100
80
60
40
20
0
12
24
36
48
60
72
Time (h)
NT siRNA
siLCLAT1-1
D
MDA-MB-231 Cas9
-Dox
+Dox
MDA-MB-231 Cas9 tet-gRNA2
C
CellTox normalized to cell confluence
20
15
10
5
E
Relative Cell Confluence
12
10
8
6
4
2
Cas9 -Dox
Cas9 +Dox
gRNA2 -Dox
gRNA2 +Dox
*

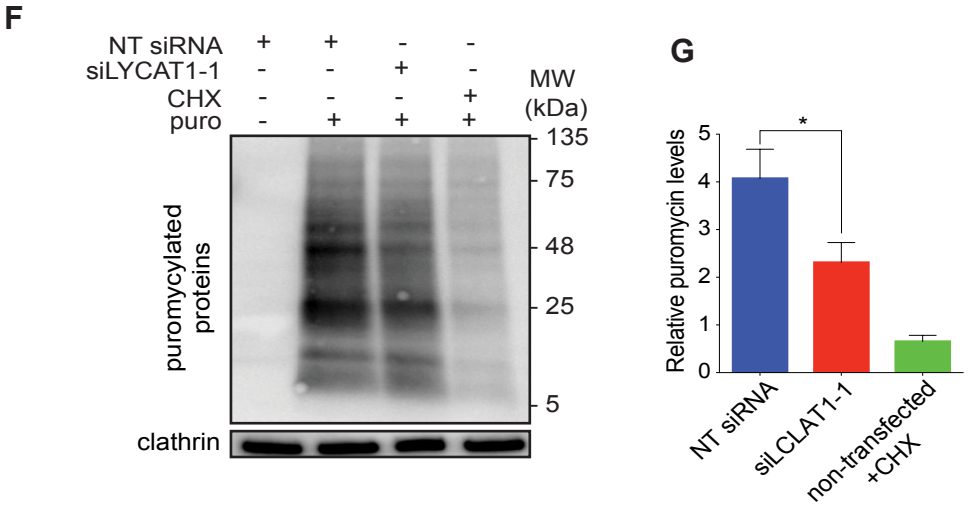
F
NT siRNA
siLYCAT1-1
CHX
puro
MW (kDa)
135
75
48
25
5
puromycylated proteins
clathrin
G
Relative puromycin levels
5
4
3
2
1
0
*
NT siRNA
siLCLAT1-1
non-transfected +CHX

Figure 8